A Study on Propeller-type Climbing Robot on Inclined Surface and its Applications

March　2023

NISHIMURA Yuki

A Study on Propeller-type Climbing Robot on Inclined Surface and its Applications

School of Integrative and Global Majors
Ph.D. Program in Empowerment Informatics
University of Tsukuba

March　2023

NISHIMURA Yuki

Abstract

A propeller-type climbing robot was studied to perform tasks on an inclined surface to reduce the burden of work currently conducted on inclined surfaces, such as walls and slopes. Conventional mobile robots cannot keep a stable attitude on inclined surfaces because the friction force applied to the robots decreases when the inclination of the surface increases. Therefore, a propeller-type climbing robot was proposed that controls the friction force by the thrust force of the multi-copter installed on the robot. The thrust force pushes the robot body against the surface and enables the robot to maintain a stable attitude on an inclined surface by producing a large friction force. When mobile robots work on tasks, they must perform some actions in an external environment with their actuators. This interaction influences the stability of the robots on inclined surfaces. In addition, for working robots that can realize stable locomotion on inclined surfaces, the efficiency of their work on tasks must be considered. The ability to navigate difficult terrain and traverse inclined surfaces depends on the steering method of the climbing robot.

The purpose of this study was to a stable condition of a propeller-type climbing robot for executing tasks on inclined surfaces, to introduce a method for managing the influence of the interaction between the actuator equipped on the robot and the environment, and to find a suitable steering method for the propeller-type climbing robot performing tasks on inclined surfaces. A model to control the magnitude and direction of the thrust force was constructed. The developed robot was evaluated in experiments on surfaces with inclination angles of 0° to 90° and various friction coefficients. Based on the stability condition of the propeller-type climbing robot, two applications are proposed for performing high-demand tasks on inclined surfaces that are usually done by humans.

The influence of the interaction between the propeller-type climbing robot and the external environment was investigated through the development of a hammering inspection robot system because the robot must move on and strike the surface during inspection. In this study, the robot was modeled under the influence of the hammering impact, an inspection robot with a novel hammering device was developed, a hammering sound classifier was implemented that works even under strong wind noise from the propellers, and the accuracy of hammering inspection by the robot was evaluated. To realize effective and efficient work on inclined surfaces with the propeller-type climbing robot, a four-wheel steering climbing robot was developed. Four-wheel steering was compared with two-wheel steering, skid steering, and mecanum wheels from the perspective of working on area coverage tasks where the robot must cover all target areas during operation. In detail, the developed propeller-type climbing robot was applied to grass-cutting tasks on inclined surfaces in hilly and mountainous areas. The robot performed grass-cutting tasks on actual sites. From a technical standpoint, this study can benefit society by providing a novel propeller-type climbing robot with four-wheel steering.

Contents

List of Figures

List of Tables

Chapter 1 Introduction

1.1 Social Background

Robots that replace humans should be designed optimally to suit environments where the robots carry out their tasks. Mobile robots that perform human tasks were developed to reduce the human labor burden and alleviate labor shortages. During the past few decades, various mobile robots have been proposed, developed, and commercialized for different uses — for example, autonomous vacuum-cleaning robots [1], robotic lawnmowers [2], and luggage-carrying robots seen in airports [3]. In addition to consumer usage, mobile robots are found in industrial environments [4] and infrastructure maintenance [5].

With mobile robots becoming widespread, they are now expected to work in more-complex environments. There are demands for mobile robots that can work on rough terrain in a harsh natural environment, work on large structures, such as bridges and skyscrapers, and work in a wide variety of environments. For example, robots that work in natural environments include mobile robots that can climb volcanoes to monitor volcanic activity [6].Grass-cutting robots have been proposed to prevent overgrown grass on slopes in hilly and mountainous areas and on the sides of highways [7]. Mobile robots that move and inspect walls and ceilings have been used to inspect and maintain concrete structures, such as bridges and high-rise structures [8]. For aerial robots, drones that monitor farmland from the sky and spray agricultural chemicals have been put to practical use [9].

As mentioned above, mobile robots are being developed to robotize work that helps humans exist and live their lives. The purpose of this research is to realize a society where humans and robots collaborate. In this dissertation, a robot that can move on steep slopes and walls is presented. The robot performed work usually done by humans — specifically, hammering inspection of structures and grass cutting on steep slopes. The hammering inspection involves interaction with the working surface, making it difficult to control the robot. In addition, grass cutting is difficult for mobile robots because it requires them to move not only on flat surfaces, such as concrete, but also on uneven grassy terrain with inclinations. In this study, a method was established for mobile robots to move on an inclined uneven surface while interacting with the environment by developing actual applications to provide a solution to the problem, which is an urgent demand in the society.

1.2 Academic Background

Realizing mobile robots that can navigate complex, uneven terrain is essential if mobile robots are to replace humans in various tasks. Working on inclined surfaces, such as steep slopes and walls, is especially challenging for robots because they must avoid slips and falls for their stable locomotion. In this section, methods to establish stable attitudes on inclined surfaces developed in previous studies to address the problem of mobile robots on inclined surfaces are explained.

1.2.1 Methods for Stable Attitude on Inclined Surfaces

The main problems encountered while moving robots on inclined surfaces are slips and falls. Previous studies have proposed different types of approach to maintain the stability of mobile robots on inclined surfaces, including steep slopes and walls. In this study, these mechanisms for traversing on inclines surfaces were categorized and investigated as follows: (1) tracked wheels or special wheels, (2) multi-legged mobile robots, (3) using wires and guide frames, (4) biomimetic methods, (5) using magnets, (6) using suction, and (7) using thrust force.

(1) Tracked wheels and special wheels

Mobile robots can be applied on steep slopes by installing tracked or special wheels with strong grips with high friction coefficients. The attempts to use this method showed improvement in locomotion on uneven terrains [10] [11]. A multi-tracked robot was developed to realize stable locomotion on steep slopes [12]. The stability of this robot was improved, but the friction coefficient was not changed by the contact area. Therefore, the maximum angle of this robot was limited to 35°. Iwano et al. [13] developed a robot with a single-tracked wheel with spikes and realized movement on a 45° slope. However, the maximum angle the robot can climb is only determined by the friction coefficient between the surface and the wheels.

(2) Multi-legged mobile robot

A six-legged robot was developed to maintain nuclear power plants and perform rescue operations after nuclear accidents [14]. Hirose et al. developed a quadrupedal robot, TITAN VII, to maintain sloped structures on highways and cut grass on the sloped side [7]. To avoid falling while performing tasks, such legged-type mobile robots keep the center of gravity close to the ground. The maximum angles that the six-legged robot and the quadrupedal robot could cover were 55° and 30°, respectively. Legged-type robots need a large number of actuators mounted on the robot, and these actuators are not only heavy but also require complicated control.

(3) Wires and guide frames

A robot that uses wire to climb mountains was proposed in Nagatani et al [6]. They developed a system that pulls a volcano observation robot with a wire [6]. ROPE-RIDE was designed as wall-cleaning robot [15]. However, wires must be prepared in advance, and the robot can only move as far as the wires can reach without getting tangled. In addition, there is the problem that the introduction cost is high when installing the guide rail on the slope.

(4) Biomimetic methods

Some studies proposed snake-like robots to realize locomotion on slopes [16] and bioinspired methods and materials [17] [18]. A snake-like robot was tested in various natural environments [16]. However, biomimetic robots tend to have limited payloads compared with wheeled mobile robots.

(5) Suction

In the suction method, adsorption to a wall-climbing robot using the pressure difference from the surroundings was investigated using a vacuum chamber by Xiao et al. [19]. However, depending on the surface shape and smoothness, there are cases when the surface and the vacuum chamber cannot be brought into close contact. Therefore, a pressure difference cannot be generated.

(6) Magnets

A robot using magnetic adhesion can generate a strong contact force. Huang et al. used a climbing robot with a magnetic tracked wheel for ship inspection [20]. The robot with a magnet showed great stability, but it can be applied only to ferromagnetic materials.

(7) Thrust force

A robot using thrust force, such as a propeller-type climbing robot, can handle inclined surfaces. The thrust force from the propeller pushes the body of the mobile robot against the surface, which generates a large friction force to keep the robot on the inclined surface. The propeller-type climbing robot has been investigated in several studies [21] [22] [23] [24] [25].

The thrust force method has the advantage of being applicable to uneven surfaces of any material. In addition to the environment-dependent parameter, which is the friction coefficient between the ground and the wheels, the robot can have a self-dependent control parameter of propeller thrust that enables the robot to maintain stability on inclined surfaces. The wheeled mobile robot with thrust force can be controlled the same way as on flat surfaces. Therefore, a robot using the thrust force method was selected in this study for replacing human tasks on inclined surfaces. However, in previous studies on mobile robots using thrust force, there have only been a few cases of applying it to actual applications.

1.2.2 Steering Methods on Inclined Surfaces

In mobile robot research, studies on locomotion on steep slopes have been limited compared with those on locomotion on flat surfaces. The ability to navigate difficult terrain and traverse inclined surfaces is critical to widening the application range of field robots. Turning is especially challenging for robots on inclined surfaces. The possible steering methods that climbing robot can use to work on tasks are (1) two-wheel steering, (2) skid steering, (3) mecanum wheels, and (4) four-wheel steering.

Skid steering is used by wheeled or tracked vehicles for their direction changes. Skid-steered vehicles experience a greater wheel slip ratio when steering than when going straight [26]. When the robot makes a right turn with skid steering, the left wheel moves forward, and the right wheel moves backward. Wheel slip occurs when the grip between the wheels and the surface decreases during sharp curves. Another option is to use a steering wheel. A steering wheel enables the robot to turn stably without losing its grip on the ground. However, the robot experiences a change in the center of gravity when it moves. A change in the center of gravity can cause the robot to fall over on a slope. Therefore, slope robots with mecanum wheels have been proposed [27] [28]. Mecanum wheels can perform holonomic motions. Therefore, the robot does not need to change the center of gravity with respect to its position. Furthermore, this robot can perform pivot turns; thus, loss of movement is minimized. Mecanum wheels have a good load-carrying capacity but have a disadvantage on an inclined or uneven surface because the mecanum wheels touch the surface incorrectly [29]. Although the wheels must touch the ground, Veerajagadheswar et al. developed a slope-cleaning robot with mecanum wheels that achieved locomotion on a slope with a 30° inclination angle [27]. Ransom et al. developed a robotic planetary rover equipped with mecanum wheels. Their robot achieved locomotion on sandy terrain with a 30° inclination. However, slips when turning on a 10° slope were reported [28]. Reina et al. [30] and Qu et al. [31] proposed a four-wheel-drive/four-wheel-steer robot to perform better on rough terrain. Corresponding experiments showed that their proposed robot could be used on all agricultural terrains. Their proposed approach was demonstrated to be effective in reducing slip and vehicle attitude errors.

The experiments on inclined surfaces have not been sufficient. Previous studies have investigated slope mobile robots focusing on stabilities on slopes and simple straight-line movement. However, stability of the robot when changing direction is also essential when working on tasks on inclined surfaces. Therefore, different locomotion methods must be evaluated to determine which is suitable for mobile robots on inclined surfaces. In addition, the robot should be evaluated regarding its coverage area for actual tasks.

1.3 Objective and Contribution

A novel attitude stabilization method and an optimal locomotion method were developed for a mobile robot that can work on inclined surfaces. A propeller-type climbing robot is based on a theory that uses thrust to push the body of the robot against a surface to stabilize its attitude. In this study, the applicability of propeller-type climbing robots to movement on inclined surfaces was examined because previous studies on propeller-type climbing robots have been limited to vertical and cylinder walls. The purpose of the study is to realize work on inclined surfaces. Therefore, the theory of a propeller robot that moves on inclined surfaces was established through the development and application of a hammering inspection robot and a grass-cutting robot for steep slopes. The first research question of this study is as follows.

Can a propeller-type climbing robot realize a stable attitude for executing tasks on inclined surfaces?

A propeller-type mobile robot that can control the magnitude and direction of thrust was modeled, and its stability conditions were clarified. In addition, conventional propeller-type mobile robots have only been able to move on concrete walls, and no consideration has been given to their performance while working. The ability to perform tasks is important for mobile robots to play an active role in human society. Therefore, this research proceeds on the premise that robots will perform work. When the robots perform work, the work actuator attached to the robot acts in some way on the external environment. Therefore, when a propeller-type climbing robot performs actual tasks, one must consider the effects of its interaction with the external environment. For example, in a hammering test, it is necessary to consider how the attitude of the mobile robot is affected by hammering. Thus, the second research question is as follows.

Is the stability of a propeller-type climbing robot influenced by interactions between the robot and the environment? If so, how should this interaction be managed?

Based on how the stability is affected when the robot performs a task, a method of controlling thrust force is proposed. After it has been confirmed that the robot can work stably, the robot must work efficiently. When it comes to actual work, it is necessary not only to aim at the destination on the surface but also to cover the target surface without omission when the robot conducts coverage area work, such as inspection, cleaning, or grass cutting. However, previous research has not validated an adequate driving method for the propeller-type climbing robot. Therefore, in this study, it was hypothesized that a propeller-type climbing robot with four-wheel steering can perform tasks on inclined surfaces effectively and efficiently. Therefore, the third research question is as follows.

Is the four-wheel steering method suitable for a propeller-type climbing robot that performs area coverage tasks on inclined surfaces?

In this study, the ability of a propeller-type climbing robot on inclined surfaces was demonstrated through the modeling of the stable condition and development of an actual robot. Moreover, the study demonstrated the capability of the robot to be incorporated into society to execute actual tasks through the development of applications.

1.4 Outline

A propeller-type mobile robot on inclined surfaces and its applications are investigated. In Chapter 1, a general introduction of mobile robot stable control and locomotion methods is provided. Moreover, the research objectives are explained. In Chapter 2, the literature is reviewed from three perspectives. First, propeller-type robots and studies on their applications are briefly explained. Then, two possible applications of the propeller-type climbing robot, hammering inspection and grass cutting on inclined surfaces, and related studies are discussed. The condition of a stable attitude on an inclined surface is modeled through numerical simulation, and the results are confirmed with a developed robot, as discussed in Chapter 3. The ability of the robot to perform hammering inspection has to be confirmed because, in hammering inspection, the robot applies force to a wall, which affects stability, as discussed in Chapter 4. The proposed robot is designed to inspect a concrete structure with a hammer strike, and the hammering sound is analyzed with a deep-learning model. In Chapter 5, another possible application, grass cutting on steep slopes in hilly and mountainous areas, is discussed. Some steering methods are compared, four-wheel steering is proposed, and its effectiveness with coverage area is confirmed. In Chapter 6, the results of this study are summarized, and limitations and future work are discussed.

Chapter 3 is based on "Development of a Steep Slope Mobile Robot with Propulsion Adhesion" in the Proceedings of the 2020 IEEE/RSJ International Conference on Intelligent Robots and Systems. Chapter 4 is based on "Automated Hammering Inspection System with Multi-Copter Type Mobile Robot for Concrete Structures" in *IEEE Robotics and Automation Letters*. Chapter 5 is based on "Grass Cutting Robot for Inclined Surfaces in Hilly and Mountainous Areas" in *Sensors*.

Chapter 2 Review of Literature

2.1 Survey of Propeller-type Climbing Robot

By comparing stabilization methods, the mechanism using a propeller can adapt to all surface shapes and materials. It can also handle heavier payloads. Propeller-type climbing robots have been reviewed previously [32]. Various mobile robots with different shapes and numbers of propellers have been developed to attach to wall surfaces using propeller thrust.

In the 1980s, Nishi et al. proposed a robot that could be used for fire extinguishing and rescue operations in fire disasters in high-rise buildings [33]. However, it was not put to practical use owing to technical limitations at the time. In 2013, Shin et al. presented a micro-aerial-vehicle-type wall-climbing robot to maintain or inspect building structures [34]. This robot pushes the wall with the propeller thrust force and moves on the wall using motor-driven wheels. In the same year, Ioi et al. developed a propeller-type climbing robot and tested its climbing ability on 45° and 90° inclination angles [35] [23]. The developed robot has a gimbal with two degrees of freedom in the center and a contra-rotating propeller. By using the thrust of the propeller mechanism as lift force and pushing the robot against the wall, movement on the wall is realized. However, theoretical consideration of the feasibility tasks on inclined surfaces has not been sufficient. In 2015, Myeong et al. [22] used quadcopter thrust to push against a wall and realized movement by motorized driving wheels on a wall for structure health monitoring, and Jung et al. [8] proposed a wind blade inspection robot. In 2017, Myeong et al. proposed a fireproof robot that can work during a fire accident [36], and they presented a control method of switching flying and climbing in 2019 [37]. Beardsley et al. [21] proposed and developed VertiGo in 2015. In 2015 and 2017, Alkalla et al. developed EJbot for inspecting concrete walls. They are attached to walls using contra-rotating propellers with greater thrust and move on walls using wheels driven by motors [25] [24]. EJbot can move on walls and cylindrical surfaces and carry a payload of 600 g when moving on walls, so its use in the real world is feasible. In 2017, Sukvichai et al. developed a robot with two propellers and four free wheels to climb a wall [38]. They concluded that propeller-type climbing robots have the potential to be used in such applications as inspection of high buildings, wall and mirror cleaning, surveillance, and military operations. In 2020, a propeller-type robot with two functions was proposed. This robot realizes the transition between the wall and the ground and perches on the wall with an arm [39].

In the aforementioned studies, only climbing on the wall, technically vertical movement on the surface, was evaluated. Consideration of lateral movement on inclined surfaces where slip occurs for mobile robots, which was raised as an issue by Iwano et al. [13], has been insufficient. Thrust control should also be considered in combination with the robot movement method. Weak thrust can cause a robot to slip, and high thrust can cause the wheels to grip too tightly and prevent the robot from turning. In addition, the loads applied to the wheels on mountain and valley sides differ. On a steep slope, the normal force applied to the wheels on a mountain side decreases, so the friction force applied to the wheels decreases, causing the wheels to slip during movement.

2.2 Survey of Applications on Inclined Surfaces

As mentioned in Section 2.1, propeller-type climbing robots have been developed for various uses, but the majority are structural inspections. Therefore, previous research on the inspection of structures is described here. Furthermore, in Chapter 1, robots that can realize work and grass cutting on slopes are in demand. Therefore, as an application example of a robot using a propeller, in this research, the realization of grass-cutting work on steep slopes by a propeller-type climbing robot was studied. To that end, previous research on grass-cutting robots is also described.

2.2.1 Review of Inspection Robots

Periodic inspections for detecting defects in concrete structures are necessary to maintain infrastructure health. During periodic inspections, surface defects, such as cracks, and internal concrete defects, such as delamination, peeling, and shallows, should be identified. Therefore, hammering tests are performed by inspectors who strike the surface manually with a hammer and detect defects by recognizing the sound produced by the hammer strikes (see Figure 2-1). Hammering inspection is a common evaluation method for detecting defects of concrete structures, such as bridges and tunnels, from sound changes [40]. However, the number of concrete structures is increasing. In addition, there is a shortage of inspectors. Therefore, it is believed that robot inspection would be beneficial. For conventional automated inspections, methods combining vision-based inspection with robots [41] [42] [43] and multi-copters [44] [45] have been proposed. There have been relatively few studies on the development and evaluation of hammering inspection robots. To realize robot hammering inspection, it is necessary to develop a mobile robot that moves on a structure stably and is not affected by the hammering impact, hammering device, and hammering defect classifier.

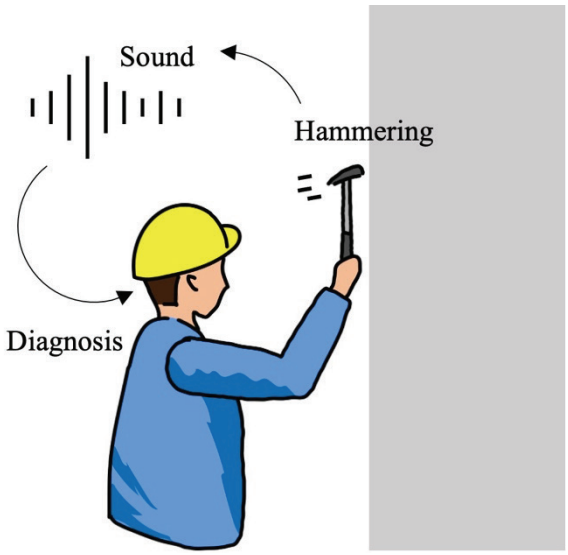

Figure 2-1 Hammering inspection.

In robotic inspection, the robot can reach areas of a concrete surface that a human inspector cannot reach, and the impact from the hammering device remains constant. In contrast, a human inspector cannot maintain a constant magnitude. In research on hammering inspection robots, robots that use wires and guide frames, as introduced in Section 1.2.1(3), are widely used. Nakamura et al. [46] and Takahashi et al. [47] constructed a guide frame along a tunnel surface, and a slider-crank hammering mechanism with an impact of 0.5 J moved along the guide frame. Luk et al. [48] developed an automated gondola-based robot equipped with a steel ball of 12 mm diameter and a linear solenoid actuator to push the steel ball to the surface. Inoue et al. [49] developed a system that detects the internal state of tiles by suspending a hammering device with a wire and lifting it. Using guide frames and cables requires system preparation before inspection and limits where wires and guide frames can be installed. In other studies using unmanned aerial vehicles (UAVs), hammering tests were conducted. Salaan et al. [50] [51] installed a solenoid-based hammering device in a UAV with a rotating shell to avoid collisions with structures. According to Ichikawa et al. [52], the impact energy of an inspector to find a defect at a depth of approximately 100 mm from the surface was approximately 0.3 J. Therefore, they developed an impact device that generates an impact with an energy of approximately 0.3 J installed on a UAV. Similarly, Moreu et al. [53] developed a UAV system with a hammering device based on a crank mechanism, and Chun et al. [54] developed a system with a piston-type impact mechanism. A UAV must always contact the surface of a structure with a constant force to strike the wall with a constant force, but controlling its flight is challenging [55] [56]. There was also a study in which suction was used, introduced in Section 1.2.1(5). Li et al. [57] developed a crawler robot with a suction cup for impact echo-acoustic inspection. They evaluated climbing ability and inspection ability separately. However, the entire inspection system was not evaluated because the climbing robot could not be applied on a vertical surface while carrying a heavy inspection device. A robot using thrust force, introduced in Section 1.2.1(7), was used for hammering inspection in research by Iwamoto et al. [58]. They developed a climbing robot that uses thrust to press its body against the tunnel surface. However, this robot was only tested for striking ability on composite panels.

In previous studies, hammer robots have demonstrated the ability to record sound by hitting the surfaces of structures. Therefore, further study on the implementation as an entire inspection system is needed. A hammering inspection system has yet to be realized by developing a mobile robot, installing a hammering device, analyzing recorded sounds, and examining the accuracy of the inspection.

2.2.2 Review of Grass-Cutting Robots

Because of the declining and aging agricultural population, agricultural robots have been developed [59] [60]. Regular grass cutting is integral to agricultural practice to prevent grass from taking essential nutrients and water away from crops. However, grass cutting by human workers is often time consuming and reduces productivity. There are data showing that small farmers in developing countries spend more than 40% of their time on grass cutting [61]. To reduce the burden of grass cutting, much research on grass-cutting robots has been conducted. For example, Bakker et al. [62] developed a grass-cutting robot for organic farms, Daniyan et al. [63] developed solar-powered mowers for gardens and parks, and Pishadory et al. [64] developed a wireless-controlled grass-cutting robot. Along with grass-cutting robots, path-planning algorithms [65] [66] [67] and obstacle prediction [68] [69] [70] for the grass-cutting robots have been studied.

Although the robots mentioned above are primarily designed for flat surfaces, grass cutting in actual farming environments is done in harsher environments. In Japan, 40% of all agricultural land is in hilly and mountainous areas [71]. According to a survey by the Ministry of Agriculture, Forestry, and Fisheries of Japan, 660 grass-cutting accidents were reported in 2000, and 29.5% of the accidents were caused by the unstable postures of workers on steep slopes [72]. The survey found that grass cutting on slopes is usually done at an angle of up to 60°, the postures of workers on slopes are unstable, and workers can slip and injure themselves while holding grass-cutting machines. Accidents are frequent in such scenarios, so there is an urgent need to replace human grass-cutting work with grass-cutting robots. Figure 2-2 shows a farmer cutting grass on a steep slope in a hilly and mountainous area.

Figure 2-2 Grass-cutting work on a steep slope.

Therefore, researchers in Japan have proposed various approaches for grass-cutting robots on steep slopes. Ito et al. [73] achieved movement on slopes of up to 30° by changing the camber angle of the robot wheels. Iizuka et al. [74] proposed a four-wheel mobile robot equipped with a wheeled arm to provide a stable attitude and realized movement on a slope of 30°. Nakatsuchi et al. [75] realized movement on a slope of up to 45° with a crawler-type robot, and Iwano et al. [13] also achieved movement on a slope of 45°. In a following study by Iwano et al. [76], they analyzed the occurrence of slippage in more detail on a 30° slope. Furthermore, Uehara et al. [77] reported on the industry–academia collaborative development of a robot that can move on slopes of up to 45°. However, in actual situations, it is necessary to cut grass on slopes of up to 60°, whereas grass-cutting work can only be performed on slopes of up to 45° with the currently developed robots. Therefore, there is still urgent demand for a robot that can handle even steeper slopes. In addition, because agriculture in hilly and mountainous areas is practiced not only in Japan but worldwide, it is assumed that there is a huge demand for robots that can reduce the burden of grass-cutting tasks.

Chapter 3　Propeller-type Climbing Robot on Inclined Surface

In Chapter 3, the stability conditions when a propeller-type climbing robot moves on inclined surfaces, including a steep slope and a wall, are formulated. Slips and falls occur when robots operate on inclined surfaces (Figure 3-1). Therefore, a method to control friction force by thrust force from a propeller was developed. The multi-copter was installed on the robot to stabilize its attitude. The thrust force pushes the robot body against the ground. As a result, the robot can keep a stable attitude on a steep slope because a large friction force is produced. Based on the stability condition of the mobile robot formulated here, the stability of the developed robot when it moves on a surface was investigated through various experiments. Specifically, the focus of this study was on controlling the magnitude and direction of the thrust force to move straight in lateral movement on inclined surfaces. In this study, vertical and lateral movements are defined as shown in Figure 3-2.

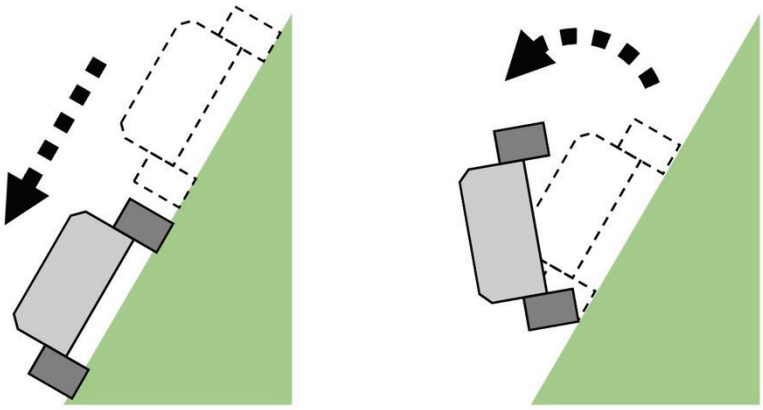

Figure 3-1 Slipping and falling on an inclined surface.

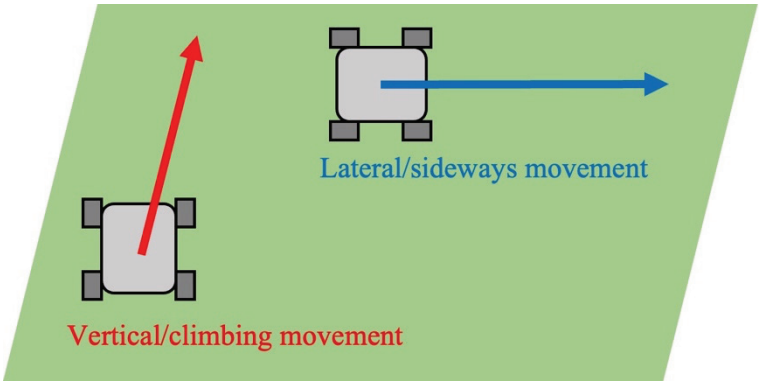

Figure 3-2 Definition of movement directions.

3.1 Stable Model of Climbing Robots on Inclined Surface

In the proposed method, the thrust of the propellers attached to the robot can push its body against the surface to increase the normal force. Therefore, the friction force increases. Consequently, the proposed robot can maintain a stable attitude without slips or falls. Figure 3-3 shows the fundamental design of the proposed propeller-type climbing robot. The robot has a quadcopter on top, a drive shaft connecting the quadcopter and the robot body with two degrees of freedom, and four motorized wheels.

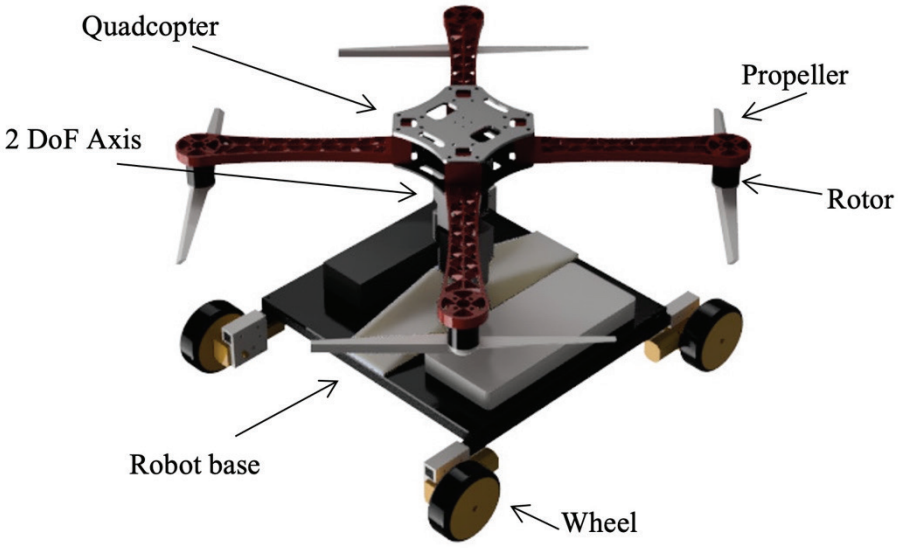

Figure 3-3 Design image of the proposed robot.

3.1.1 Stabilization Models

Stable Condition Against Slips

The relationship between the friction force and the downward force acting on a robot on inclined surfaces was analyzed. Figure 3-4 shows a force diagram of a robot without the proposed method, and references to the robot wheel positions are labeled. Assuming that the acceleration of gravity is g, the friction coefficient between the ground and the wheels is μ, and the slope angle is θ, the mass of the climbing robot is m. The gravity force mg can be divided into a downward and a vertical force to the surface. The friction force is proportional to the total normal force of $N_{upper\text{-}right}$, $N_{upper\text{-}left}$, $N_{lower\text{-}left}$, and $N_{lower\text{-}right,}$ which are the normal forces applied to the upper-right, upper-left, lower-left, and lower-right wheels, respectively. Therefore, the friction force $F_{friction}$ is written as

$$F_{friction} = \mu N_{upper-right} + \mu N_{upper-left} + \mu N_{lower-right} + \mu N_{lower-left} \tag{3.1}$$

If the friction force acting on the robot is greater than the downward force, the robot does not slip. Thus, the stable condition for the climbing robot not to slip on the surface with inclination angle θ is

$$F_{friction} \geq mg \sin\theta \tag{3.2}$$

This condition can be written in a different form without Ns as

$$\mu\, mg \cos\theta \geq mg \sin\theta \tag{3.3}$$

As the angle of inclination increases, the downward force increases, but the vertical force decreases. The friction force is proportional to the normal force, so the greater the inclination, the less the friction force. Therefore, the moving robot on the slope does not satisfy Equation (3.3), and the robot slips on the surface.

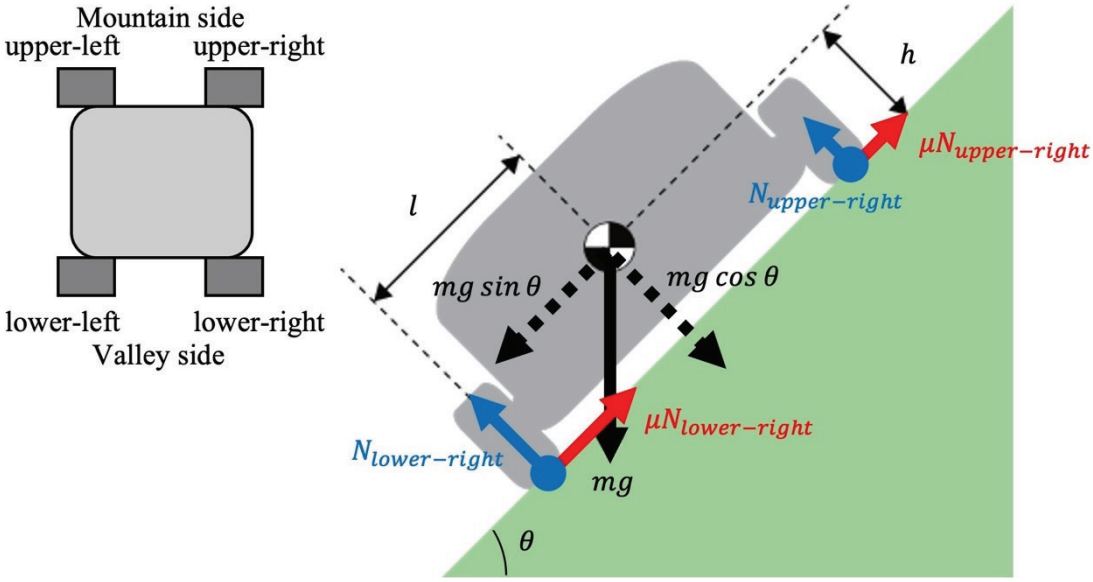

Figure 3-4 Force diagram of the robot without the proposed method.

The proposed robot pushes the robot body with thrust force F_p with a thrust tilted at angle ϕ to the ground, as shown in Figure 3-5. The thrust inclination angle when the propeller is tilted to the valley side is defined as positive. The downward force is reduced with the sinusoidal component of the thrust force, and the friction force increases with the cosine component of the thrust force. Therefore, the stable condition of the proposed robot can be written as

$$\mu \left(N_{upper-right} + N_{upper-left} + N_{lower-right} + N_{lower-left}\right) \geq mg \sin\theta - F_p \sin\phi \tag{3.4}$$

This condition can be written in a different form without *N*s as

$$\mu \left(mg \cos\theta + F_p \cos\phi\right) \geq mg \sin\theta - F_p \sin\phi \tag{3.5}$$

From Equations (3.3) and (3.5), compared with the case in which the proposed method is not used, the proposed mobile robot can maintain a stable attitude on surfaces with a larger inclination angle. When the thrust force pushes the robot body with a tilted angle with respect to the ground, the thrust force increases the friction force and reduces the downward force that causes the robot to slip on the inclined surface.

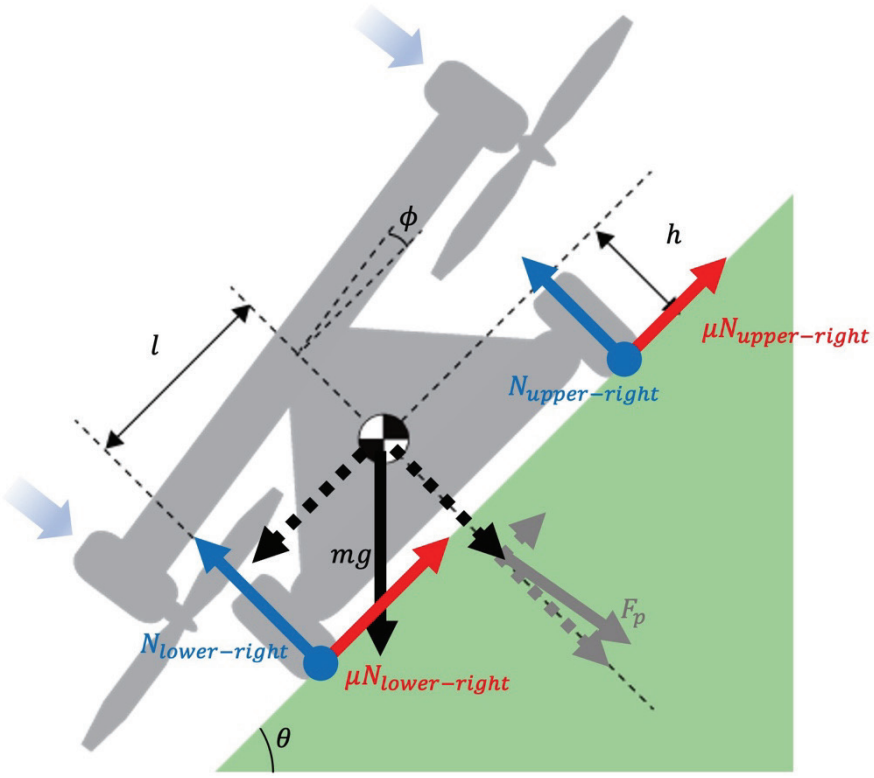

Figure 3-5 Force diagram of the robot with the proposed method.

Stable Condition Against Falls

The moment causes the fall of the mobile robot. The lower wheel is defined as the center of the moment, and the moment is in a clockwise direction. Here, h is the height from the ground to the robot center of gravity, l is the length from the lower wheels to the robot center of gravity, and L is the width of the robot. When the robot does not fall on an inclined surface, the moment acting on the mobile robot must meet the following condition.

$$lmg\cos\theta - hmg\sin\theta - L(N_{upper-right} + N_{upper-left}) \geq 0 \tag{3.6}$$

where $N_{upper\text{-}right}$ and $N_{upper\text{-}left}$ are the normal forces of the upper-right and upper-left wheels, respectively. If Equation (3.6) is not satisfied, $N_{upper\text{-}right}$ and $N_{upper\text{-}left}$ are negative, the upper wheel leaves the ground, and a fall occurs. If the mass of the robot is large, it can obtain a large vertical force from that mass, but it is difficult to maintain a stable attitude because of the increased downward force.

When the proposed method is used, the moment acting on the robot must satisfy

$$lmg\cos\theta - hmg\sin\theta - L(N_{upper-right} + N_{upper-left}) + lF_p\cos\phi - hF_p\sin\phi \geq 0 \tag{3.7}$$

Here, when the range of ϕ is 0° to 45°, and l is larger than h, the left side of Equation (3.7) is larger than the left side of Equation (3.6); therefore, a mobile robot using the proposed method is more resistant to falls than a normal robot without the proposed method. Based on Equation (3.6), a legged-type climbing robot was designed to satisfy the stability condition against falls by moving the robot center of gravity closer to the ground and to the upper side of the inclined surface. However, the robot center of gravity is determined by its design. Even if the stability against falls is increased by moving the center-of-gravity position, the stability conditions against slips cannot be improved. By using the proposed method, it is possible to prevent slips and falls to realize work on inclined surfaces.

From Equation (3.7), the normal forces applied on the robot are

$$N_{upper-right} = N_{upper-left} = \frac{1}{2}\left\{\frac{mg}{L}(l\cos\theta - h\sin\theta) + \frac{F_p}{L}(l\cos\phi + h\sin\phi)\right\} \tag{3.8}$$

$$N_{lower-right} = N_{lower-left} = \frac{1}{2}\left\{\frac{mg}{L}(l\cos\theta + h\sin\theta) + \frac{F_p}{L}(l\cos\phi - h\sin\phi)\right\} \tag{3.9}$$

As shown in Equations (3.8) and (3.9), the normal forces acting on the upper and lower sides of the wheels have different values. This means that the wheels on the upper side only can generate a smaller driving force than the wheels on the lower side because of the relationship between friction force and driving force. In the following sections, the locomotion ability to avoid unexpected slips on inclined surfaces is discussed.

3.1.2 Evaluation with a Simulation

In this study, a mobile robot with the proposed propeller stabilization was modeled, and the relationship between the thrust force, mass of the robot, and inclination angle was clarified by simulation using a physics engine. Physics simulations were performed using the Bullet Real-Time Physics Simulation [78] and Open Dynamics Engine [79] on V-REP [80]. The physics model was created to simulate the proposed climbing robot with five rigid bodies: a robot body, four drive wheels, a propeller base, four propellers, and a connection part. The simulated thrust force of the propellers was applied evenly to the center of the four propellers shown in Figure 3-6. The weight of the mobile robot was 1.5 kg at the initial point, and the center of gravity was set to the center of the robot.

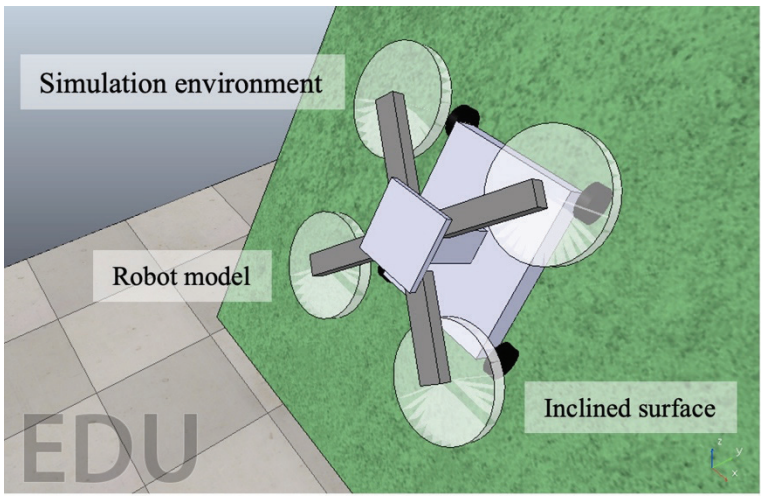

Figure 3-6 Simulation environment.

Maximum Stable Angle

It was confirmed that the proposed method improves the maximum surface inclination angle at which the mobile robot can maintain its attitude. Here, the maximum stable angle is defined as the inclination angle of the surface where a robot can maintain the attitude without slips and falls. The inclination angle was increased from 0° to 90° in 0.1° increments in the numerical simulation. The wheel was fixed to be locked in rotation, and the direction of the wheel was not considered.

First, the simulation experiment was conducted when the friction coefficient was increased, as introduced in Section 1.2.1(1). The mass of the robot was fixed at 1.5 kg. Figure 3-7 shows the maximum stable angle and friction coefficient relationship. When the friction coefficient was small, the mobile robot slipped when the inclination angle increased. If the friction coefficient exceeded a certain value, a fall occurred before the slip occurred. Therefore, the maximum stable angle became constant, even with the increase in the friction coefficient.

Next, the simulation considered the case in which the proposed method was used. The change in maximum stable angle was observed when the thrust force was changed from 0 to 20 N in 5.0-N increments, the thrust tilted angle was fixed at 0°, and the friction coefficient was fixed at 1.0. The result is shown in Figure 3-8. Even if the mass of the robot is increased, the maximum stable angle can reach 90° with the appropriate selection of thrust force. Because the mass of the robot increases when the thrust is 0 N, the friction force should also increase, but there is no benefit in maximizing the stable angle because the downward dragging force increases simultaneously. When the friction coefficient is large, the increase in thrust force generates a larger friction force, increasing the maximum stable angle. In conclusion, mobile robots exert a greater effect not only by increasing the thrust force but also by combining it with the conventional method of increasing the friction coefficient of the wheels.

Finally, the change in the direction of the thrust force was examined. From the stable condition, the thrust tilted angle affects the maximum stable angle. In the simulation, the thrust tilted angle was set to 0° to 45° in 5° increments. The results are shown in Figure 3-9. The magnitude of the thrust was 0 N, 10 N, 20 N, and 30 N. When the thrust force was large enough, the robot could maintain a stable attitude on a surface with an inclination angle of 90°, regardless of the thrust tilted angle. Then, in the case in which the thrust magnitude was 10 N and the thrust was 20 N, the change in the direction of thrust positively affected the maximum stable angle. The effect of the thrust direction on the maximum stable angle was smaller in the case of 10 N than in that of 20 N. It was shown that choosing the appropriate value of the thrust tilted angle greatly benefits the maximum stable angle that can maintain the attitude.

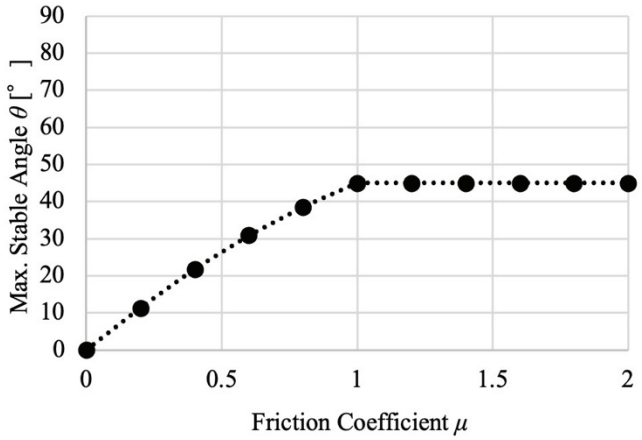

Figure 3-7 Friction coefficient versus maximum stable angle.

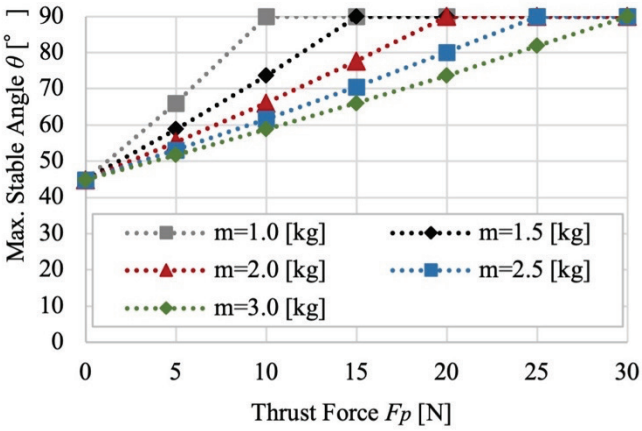

Figure 3-8 Thrust force versus maximum stable angle with different mass values.

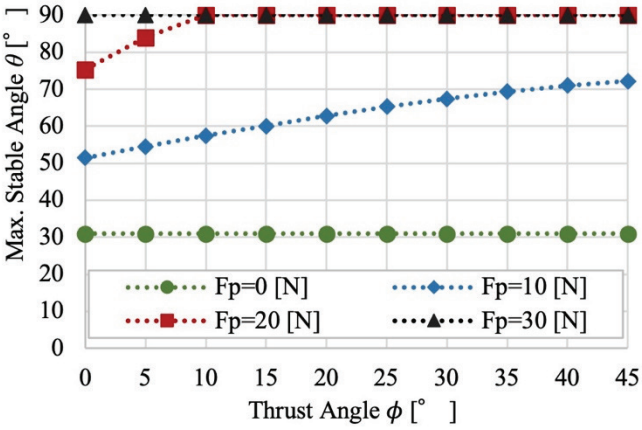

Figure 3-9 Thrust tilted angle versus maximum stable angle with different thrust force values.

Climbing Ability

Because the proposed propeller-type climbing robot works on inclined surfaces, its climbing ability was also examined through simulation. The maximum angle at which the robot can climb upward on the surface was measured when the torque of the wheels and thrust force were changed. The torques applied to the wheels were 0.1 Nm, 0.25 Nm, 0.5 Nm, 0.75 Nm, and 1.0 Nm. The inclination angle was increased by 10° from 0° to 90°. The results are shown in Table 3-1. In the case in which only the torque of the wheel was changed, the maximum inclination angle of the surface that the robot could climb was up to 40°. Increasing the torque of the wheels did not improve the climbing ability of the robot. This is because the torque transmitted by the wheel to the ground depends on the friction force. It is necessary to increase the torque and friction force simultaneously.

With the proposed method, the friction force generated by the robot can be increased by the presence of thrust force. It is necessary to investigate whether the climbing ability increases when the friction force is increased by using the proposed method. Therefore, the improvement in the climbing ability using the proposed method was evaluated. The magnitude of the thrust force was set from 0 N to 20 N in 5 N increments. The inclination angle of the surface was changed by 10° from 0° to 90°, the torque of the wheels was 0.25 Nm, the friction coefficient was 1.0, and the thrust tilted angles were 0° and 20°. The results are shown in Table 3-2 and Table 3-3. It was confirmed that the proposed propeller-type climbing robot can climb surfaces up to 90° when the direction of thrust force is controlled. Pushing the robot body to the surface increased the friction force applied to the wheels, and a large driving force could be generated, enabling the robot to climb a surface with a large inclination angle. Therefore, the direction of thrust is significantly related to the maximum inclination angle at which the attitude of the robot can be maintained. To maximize the maximum stable inclination angle and climbing angle, the magnitude of thrust force and its tilted angle should be controlled appropriately.

Table 3-1 Maximum climbing angle with different wheel torques.

Torque [Nm]	0.1	0.25	0.5	0.75	1.0
Maximum Climbing Angle [°]	30	40	40	40	40

Table 3-2 Maximum climbing angle with different thrust forces (ϕ = 0°).

Thrust Force [N]	0	5	10	15	20
Maximum Climbing Angle [°]	30	50	60	70	80

Table 3-3 Maximum climbing angle with different thrust forces (ϕ = 20°).

Thrust Force [N]	0	5	10	15	20
Maximum Climbing Angle [°]	30	60	70	90	90

3.2 Design and Fabrication

3.2.1 Developed Robot

Figure 3-10 shows the robot developed to confirm the stable condition of the propeller-type climbing robot introduced in Section 3.1. The robot uses a quadcopter that generates a maximum thrust of 20 N, with four DJI E305 2312E motors (960 kV) to rotate the propellers and four DJI E305 420 Lite ESC systems for electronic speed control (ESC) to control the rotor speed. The robot frame was made of aluminum pipes to reduce weight, and a DC motor was used for the driving wheels. Each actuator was controlled using Microchip's Atmega328p. The LiPo battery (1800 mAh, 11.1 V, 150 g) and the control unit were attached to the base of the robot because the center of gravity affects its stability against falls. To enable the developed robot to achieve any desired thrust tilted angle, a mechanism with two degrees of freedom consisting of two servo motors at the connection between the quadcopter and the robot body was installed. With this mechanism, the thrust force could be tilted from −20° to 20° in any direction. The width, height, and depth of the developed robot were 270 mm, 210 mm, and 300 mm, respectively. The robot weight was 1.55 kg. A triaxial acceleration sensor for measuring the inclination angle of the surface was attached. In addition, a loadcell was attached to the wheels to monitor the pushing force of the thrust of the propeller.

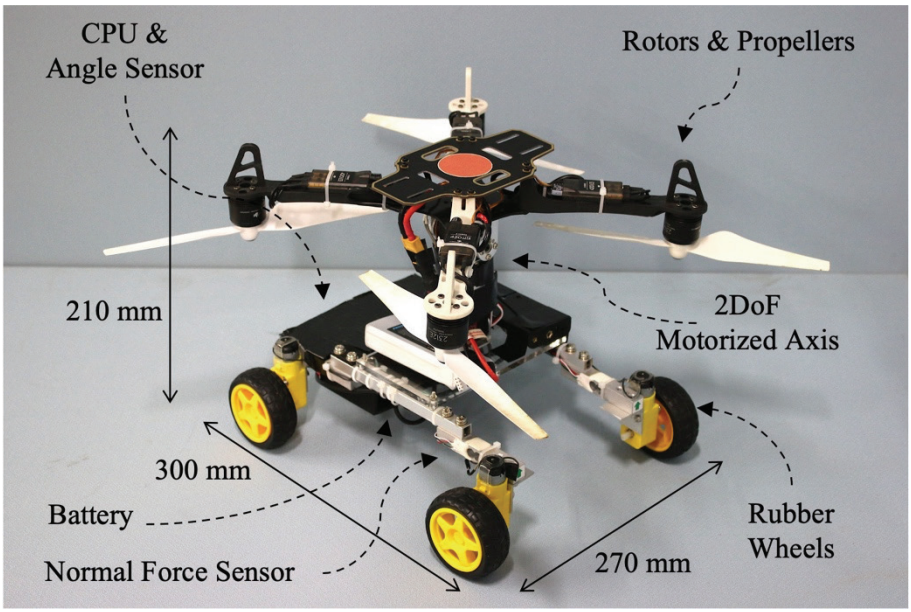

Figure 3-10 Developed propeller-type climbing robot (prototype).

3.2.2 Control Strategy

A strategy for controlling the thrust forces was developed. In the proposed method, the thrust of the propeller pushes the robot body against the slope. However, the magnitude of the thrust force required is small on a surface with a gentle inclination and becomes larger on a steep inclination. To generate a large friction force by using a constant thrust force to push the robot is not a problem when only the stability of the attitude is considered. However, the constant force requires significant battery consumption, even on a gentle inclination, which is a critical issue for a robot driven by a battery. Therefore, the developed robot controls the propeller according to the inclination angle.

In this study, the inclination angle was obtained in real time from the equipped angle sensor, while the friction coefficient was measured in advance. The required thrust was calculated based on these two parameters, then the rotation speed of the rotors was controlled. Figure 3-11 illustrates the relationship between the thrust force and the tilted angle on the rubber surface with three different inclination angles. The green area corresponds to the conditions for avoiding slips described in Equation (3.5). The blue area corresponds to the condition that satisfies Equation (3.7) — the condition for not falling. The red area shows the ratio of the load applied to each wheel. The red area indicates when the ratio of wheel loads on the upper and lower sides of the inclined surface is satisfied, written as

$$\delta = \frac{N_{upper-right} + N_{upper-left}}{N_{lower-right} + N_{lower-left}} \tag{3.10}$$

The ratio was targeted to 0.5 or more and 1.0 or less to avoid unexpected slips on inclined surfaces. The black line represents the mechanical limitations of the developed robot. The magnitude and angle of thrust were selected from the overlapping areas of the three areas where the robot can achieve stable movement.

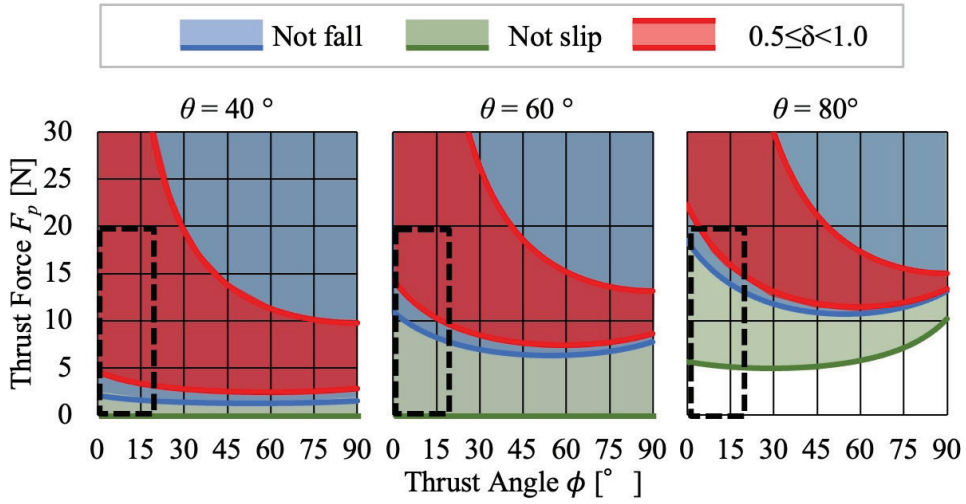

Figure 3-11 Example of thrust force control strategy (μ = 0.71).

3.3 Experiment and Result

The stability of the developed robot on a slope was evaluated through fundamental stability, climbing, and lateral movement evaluation experiments. In previous studies, robots developed to move on rough terrains, such as steep slopes and walls, have been evaluated on rubber sheets, concrete walls, and artificial grass. In this study, the experiment was conducted on concrete, a rubber sheet, and artificial grass, as shown in Figure 3-12. The slope with any angle was realized by a wooden board and frames, as shown in Figure 3-13. Table 3-4 shows the friction coefficient between each surface and the wheel of the developed robot.

Table 3-4 Friction coefficients of surface materials.

Surface	**Friction coefficient**
Rubber	0.71
Concrete	0.96
Artificial grass	0.62

Figure 3-12 Surface materials (concrete, rubber, artificial grass).

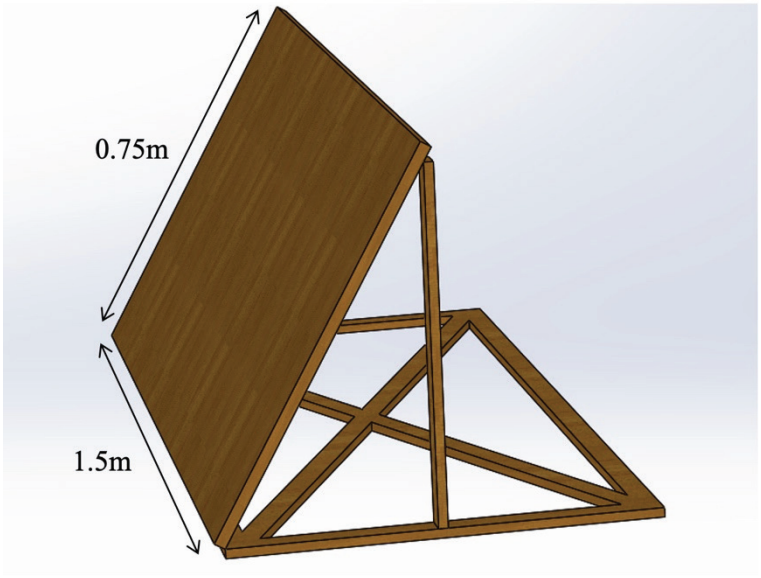

Figure 3-13 Slope realized by a wooden board and frames.

3.3.1 Stability Evaluation

An experiment was conducted to evaluate the attitude maintenance of the developed propeller-type climbing robot with respect to the maximum inclination angle. The robot was installed on a flat plane. The angle of the plane on which the robot was installed was gradually increased from 0° to 90°. As the inclination angle increased, the robot slipped or fell, and the maximum stable inclination angle without slips and falls was recorded. First, the thrust forces were controlled to be 0 N and 20 N, and the experiment was conducted while the thrust force remained constant. When the output of the thrust force was 20 N, experiments were performed on two thrust tilted angles of 0° and 20° (see Table 3-5). It was confirmed that the attitude of the robot with the proposed method could be maintained, while that of the robot without it could not. The maximum stable inclination angle was further increased when the thrust force was tilted. The experimental results are almost identical to the results of the simulations.

Table 3-5 Maximum stable angle on three different surfaces.

Force [N]	**Thrust tilted angle [°]**	**Concrete [°]**		**Rubber [°]**		**Artificial grass [°]**	
		Exp.	Cal.	Exp.	Cal.	Exp.	Cal.
0	0	40.5	43.8	37.5	35.3	35.5	31.7
20	0	90	90	80	87.2	78.5	77.5
20	20	90	90	90	90	90	90

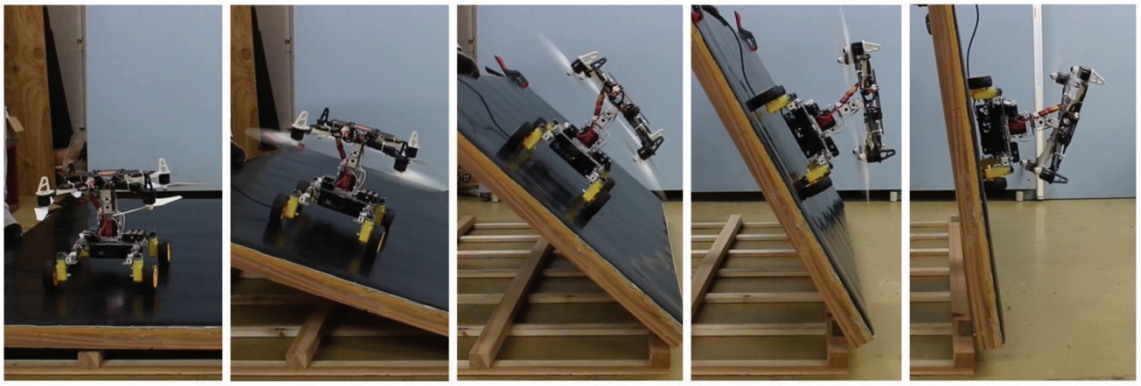

Figure 3-14 Stability evaluation on the rubber surface.

A study was conducted to confirm whether the developed robot could control the output of the magnitude of thrust and its tilted angle by inputting the inclination angle of the surface measured by the sensor. As in the abovementioned experiment, the robot was installed on a flat plane, and the angle of the plane was gradually increased. Figure 3-14 shows the robot on different slope angles during the experiment. Figure 3-15 shows the values from the angle and normal-force sensors. Figure 3-16 shows the thrust and thrust tilted angle values output during the experiment. The estimated value of normal force in a case where the proposed method was not used was calculated using the measured inclination angle with Equations (3.11) and (3.12).

$$N_{upper} = \frac{mg}{L}(l\cos\theta - h\sin\theta) \tag{3.11}$$

$$N_{lower} = \frac{mg}{L}(l\cos\theta + h\sin\theta) \tag{3.12}$$

where, N_{upper} is the estimated normal forces applied on the upper wheels without the proposed method, and N_{lower} is the estimated normal forces applied on lower wheels without the proposed method. Here, N'_{upper} is the total value of the measured normal forces applied on the upper wheels, and N'_{lower} is the total value of the measured normal forces applied on the lower wheels.

As a result, on a gentle inclination, the robot can maintain its attitude without the proposed method, so no thrust is generated. When the inclination angle increases, the friction force and moment acting on the robot are insufficient, causing slips and falls. To compensate for the lack of friction force, the magnitude and direction of the thrust force are increased. There is no noticeable difference between the measured normal forces on the upper and lower sides of the wheels. However, there is a large imbalance in the estimated normal force on the upper and lower sides of the wheels without the proposed method, represented by the dashed line. Setting the thrust tilted angle to 0° adds the normal forces evenly to both sides of the wheels. Thus, it is impossible to reduce the gap between the two normal forces on the upper and lower sides of the wheels. However, when the proposed method is used, each wheel of the mobile robot can generate approximately the same amount of driving force to realize stable movement on an inclined surface.

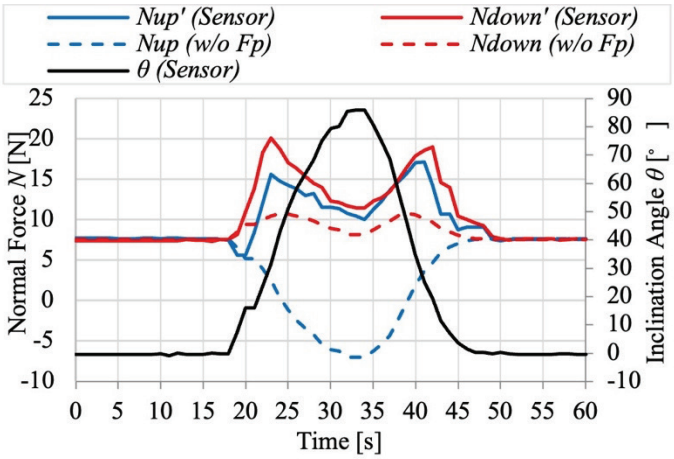

Figure 3-15 Time versus measured inclination angle and normal forces.

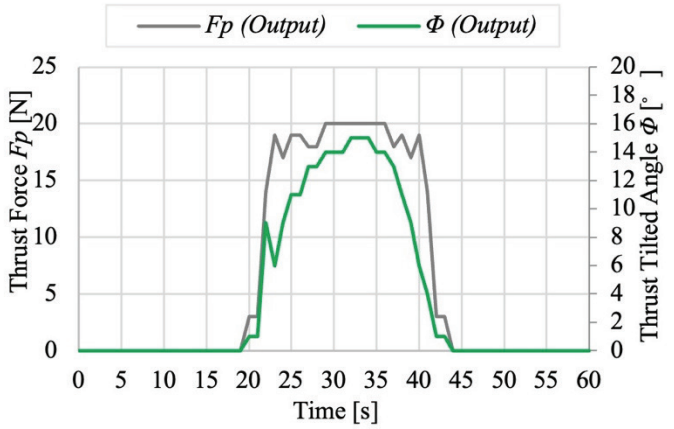

Figure 3-16 Time versus output of thrust force and tilted angle.

3.3.2 Climbing Evaluation

The climbing ability of the developed robot was evaluated to confirm that the robot has sufficient torque to move on an inclined surface and transmit sufficient driving force to the surface. In the experiment, the thrust force was 20 N, and the thrust tilted angle was 20°. The results show that the developed robot could climb all three material surfaces with an inclination angle of up to 90° (see Figure 3-17).

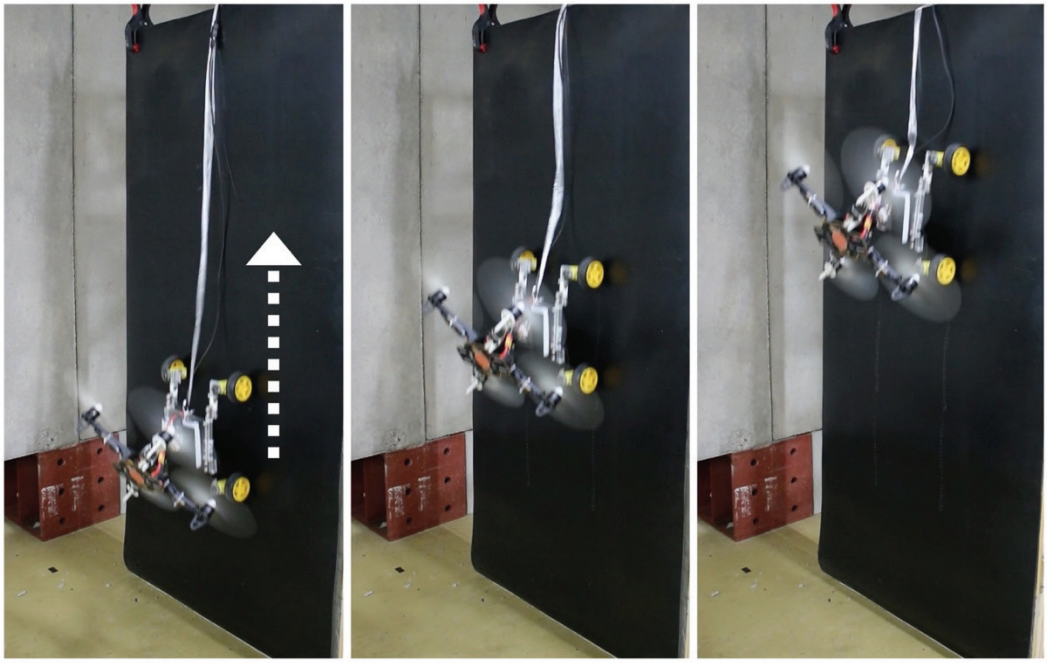

Figure 3-17 Fundamental climbing experiments.

3.3.3 Navigation Evaluation

In this experiment, the path of the robot when moving sideways on a slope was observed. A rubber sheet was used as the material of the surface, and the inclination angles were set to 20°, 40°, 60°, 80°, and 90°. In addition, when the inclination angle was 60°, the concrete and artificial grass were also tested as surface materials for comparison. The locomotion on a 60° surface with rubber, concrete, and artificial grass is shown in Figure 3-18, Figure 3-19, and Figure 3-20, respectively.

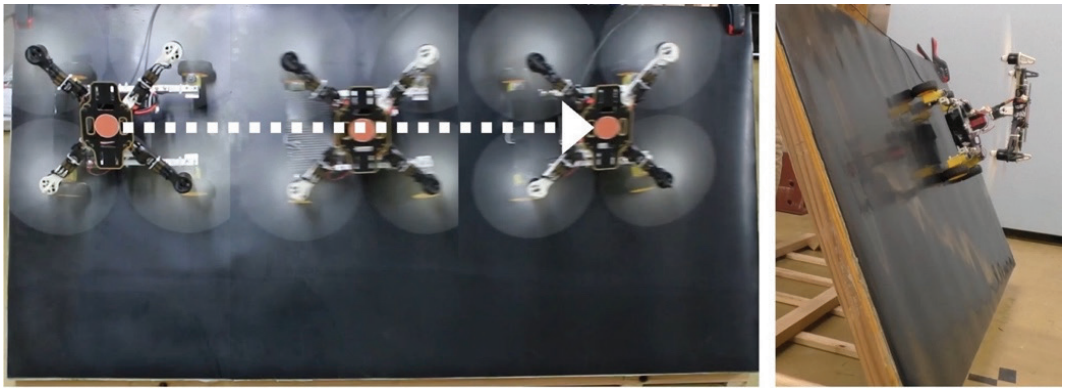

Figure 3-18 Lateral movement experiment on the rubber surface.

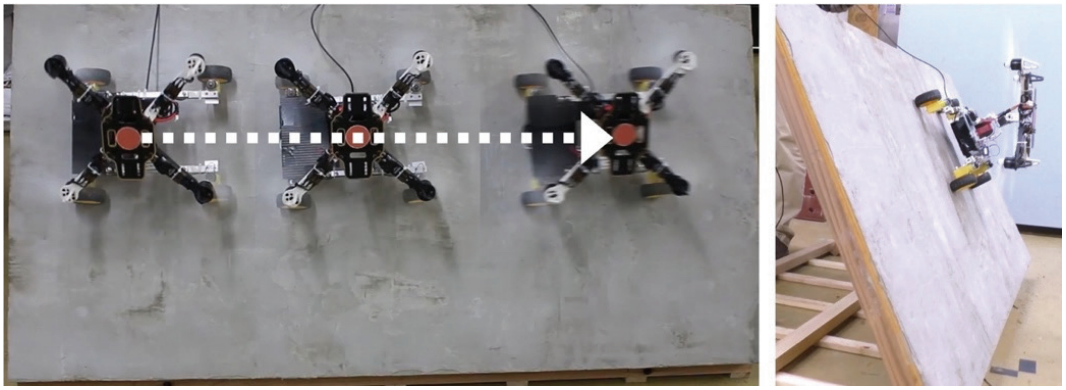

Figure 3-19 Lateral movement experiment on the concrete surface.

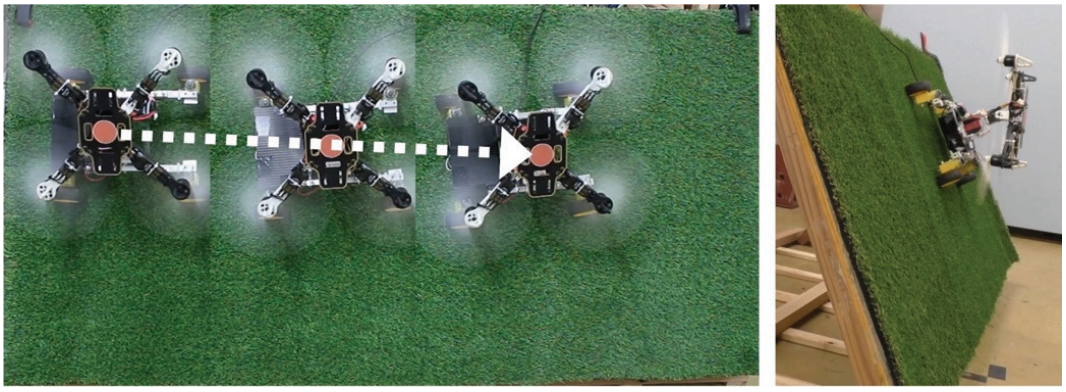

Figure 3-20 Lateral movement experiment on the artificial-grass surface.

The paths of the robot during the experiment on a rubber surface with inclination angles of 20°, 40°, 60°, 80°, and 90° are shown in Figure 3-21. The robot could not realize stable movement with an inclination angle of 40° without the proposed method. When the thrust force was 20 N, and its tilted angle was 20°, the robot could move on an inclined surface with an inclination angle of up to 90° without any slips or falls. A slight slip was observed on the artificial-grass surface, even when the thrust force was 20 N and the tilted angle was 20°. This is because artificial grass has a considerable variation in friction coefficient. The magnitude of the thrust force and the thrust tilted angle was calculated based on the average friction coefficient. An unexpected slip occurred if the friction coefficient between the artificial grass and the robot wheel reached less than the average. Safety factors, such as additional thrust force, are required on uneven surfaces, such as grassy terrain to prevent slips.

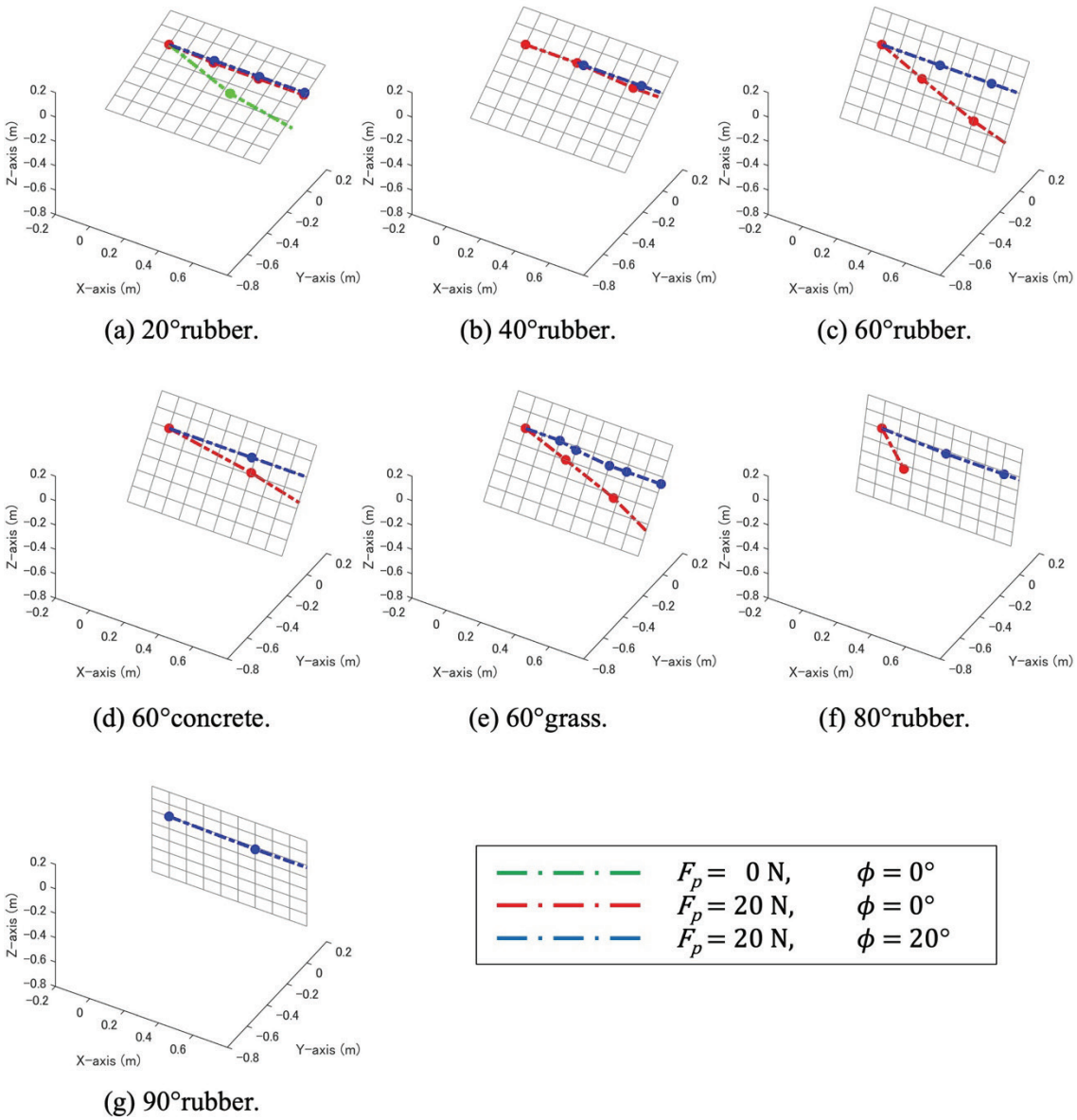

(a) 20°rubber. (b) 40°rubber. (c) 60°rubber.

(d) 60°concrete. (e) 60°grass. (f) 80°rubber.

(g) 90°rubber.

Figure 3-21 Paths of the robot in lateral movement experiments.

3.4 Discussion

Because mobile robots that move on inclined surfaces must overcome slips and falls, research on mobile robots that can work on inclined surfaces has been lacking compared with working robots on flat surfaces. In Chapter 3, the propeller-type climbing robot, a mobile robot that uses propeller thrust force, was formulated with stability conditions. The proposed mobile robot was modeled by simulation, and the behavior of the mobile robot on inclined surfaces was analyzed. The effectiveness of the proposed method, pushing the robot body against the surface by thrust force with the tilted angle to generate a large friction force, was confirmed. To ensure stable movement, the influence of the driving force generated on the wheels when climbing a slope and the ratio of the normal force acting on the wheels on the upper and lower sides of inclined surfaces were studied. A mobile robot that realizes the proposed method was developed. The experimental results revealed that, when the magnitude and direction of the thrust force are controlled, the developed robot can maintain a stable attitude and locomotion on different materials with an inclination angle of up to 90°.

One limitation of the developed robot is the operating time. Because the robot is run on a battery, the operation time is determined by the size of the battery. The theoretical operation time is long when the robot is on a gentle slope with a large friction coefficient. The running time is shorter if the robot moves on a surface with a large inclination and a small friction coefficient. For example, when moving on a concrete surface at 40°, the theoretical operation time is more than 20 min. Moving on a surface of artificial grass at 80°, the operation time is less than 5 min.

A working robot that can perform tasks on inclined surfaces is necessary to carry out tasks on actual surfaces. Depending on the type of task, interaction with the environment is required while moving on surfaces. Then, the reaction force can cause the robot attitude to become unstable. In addition, it is necessary to consider the work actuator mounted on the work robot and clarify the relationship between the change in the weight loaded on the mobile robot and its stability. When realizing work in an actual environment, the friction coefficient between the ground and the wheels changes, and the propeller-type climbing robot must overcome the unevenness of the terrain. Even in such an environment, the robot is required to perform tasks with stable locomotion. The steering method of a propeller-type climbing robot should be examined to realize optimal stable movement in an actual environment when using the proposed method.

Chapter 4 Application 1: Hammering Inspection

4.1 Overview of Hammering Inspection System

In previous studies, conventional climbing robots designed to perform hammering inspection have been evaluated only in terms of stability and locomotion on concrete walls, and no consideration has been given to when they perform an actual inspection. When robots perform hammering inspection, the hammering device attached to the robot strikes the wall. The propeller-type climbing robot must consider the effects of the reaction force from striking on the stability. Through the development of a hammering inspection system as an application of a propeller-type climbing robot, how the influence of the interaction between the robot and the environment should be managed was clarified.

4.1.1 Introduction of Proposed Hammering Inspection Robot

As shown in Figure 4-1, an automatic hammering inspection system with a hammering device, sound- and image-collecting functions to record the positions of defects on concrete structures, acoustic analysis, and result plotting was developed. The robot moves on the concrete surface freely, and a microphone records the sound when the hammer strikes the surface. A camera records the position of the robot. Sound and images are used to detect defects. The proposed system has all the functions necessary to conduct a hammering inspection.

To perform the hammering inspection, the propeller-type climbing robot must hit the surface of the structure and collect the hammering sound. Therefore, a unique actuator and mechanism that generate enough impact force on the surface were designed.

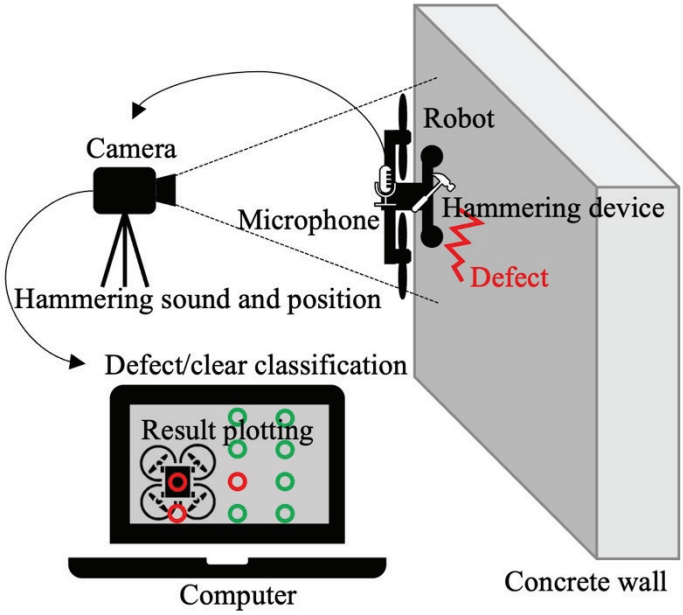

Figure 4-1 Robot hammering inspection system.

4.1.2 Stability of Inspection Robot on Walls

A propeller-type climbing robot uses thrust force to keep its position on the wall so that the distance between the robot and the wall surface remains constant. Furthermore, the propeller-type climbing robot can touch the wall with a constant contact force. As explained in Section 3.1, the propeller-type climbing robot has two stability conditions: friction force and moment. The model in Section 3.1 corresponds to surfaces with inclination angles from 0° to 90°, but the case where θ is 90° was only considered for the inspection robot for a concrete wall. Based on the basic stability conditions described in Section 3.1, the stability conditions were extended to a hammering inspection robot that performs its tasks on walls. In the force diagram shown in Figure 4-2, the propeller thrust forces on the upper and lower sides are written as $F_{p\text{-}upper}$ and $F_{p\text{-}lower}$, respectively. The normal forces acting on the upper and lower wheels are N_{upper} and N_{lower}, respectively. The distances from the surface to the center of mass and the propellers are h_{COG} and h_p, respectively. The distance from the center of gravity to the wheels in the vertical direction is l_{COG}. The distance from the lower wheels to the lower propellers is l_p. The reaction force of the hammering impact applied to the robot includes a stable condition. The average impact force per unit time is defined as F_i. The stable state of friction and moment is described as

$$\mu(F_{p-upper} + F_{p-lower} - F_i) > mg \tag{4.1}$$

$$-F_{p-upper}l_p - mgh_{COG} - 2N_{lower}l_p + F_{p-lower}(2l_{COG} + l_p) - F_i l_{COG} \geq 0 \tag{4.2}$$

Equation (4.2) shows that the negative moments should be avoided to stabilize the robot. To reduce the influence of the moment, the mass of the robot was reduced. Furthermore, to reduce the influence of the moment, the battery position was lowered. An attempt was made to include the impact force of the robot in stable condition by clarifying the relationship between the average hammering force and the thrust force. These conditions were used to design the robot described in the following sections.

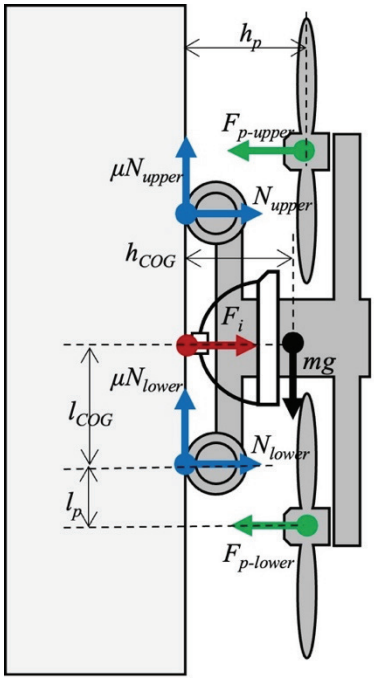

Figure 4-2 Force diagram of proposed hammering inspection robot.

4.2 Design and Fabrication

4.2.1 Hammering Device

A lightweight hammering mechanism to be mounted on climbing robots was developed. The hammering device has a simple mechanism that uses a snap motor that provides a strong and quick impact on a concrete surface. Before the device was mounted on the robot, fundamental hammering experiments were performed on concrete test blocks.

Development of Hammering Device

An actuator consisting of a spring metal strip that rotates one end of a metal strip while the other side of the metal strip is fixed was adopted as an actuator for a hammering device to generate a rapid and strong impulse force [81]. This actuator is lightweight and easy to mount on an inspection robot. Usually, a small actuator cannot produce enough of an impact, but the developed hammering device achieved the same kinetic energy as the hammering of an inspector. Figure 4-3 shows the developed hammering device. The metal strip was used as a spring, the device frame was printed with polylactic acid (PLA) by a 3D printer, and an MG92B servo motor was used to rotate one end of the metal strip. The length, width, and thickness of the metal strip were 200 mm, 30 mm, and 0.15 mm, respectively. The diameter of the steel ball was 10 mm, and the mass was 4 g. The total mass of the hammer section, consisting of the hammerhead, a metal strip, and screws, was 17 g. The total weight was 60 g.

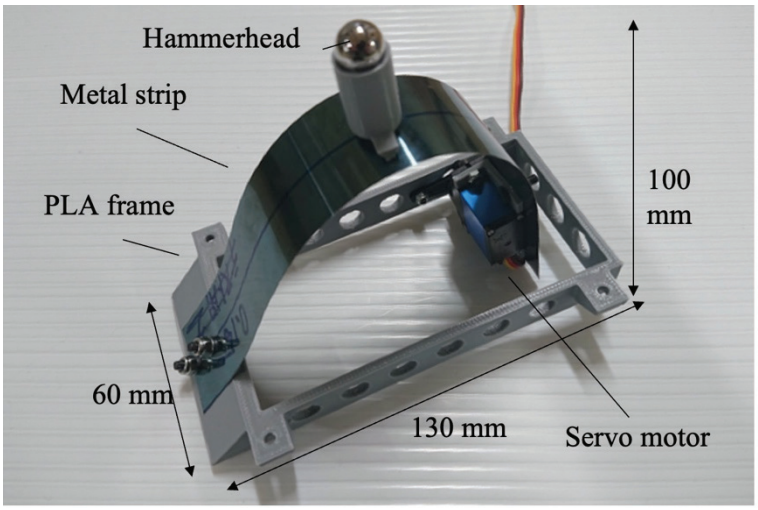

Figure 4-3 Developed hammering device.

Fundamental Experiment

Figure 4-4 shows a series of hammering sequences performed by the developed hammering device. First, the servo motor rotated, and the metal strip bent slowly. Then, after the servo motor reached a certain angle, the deformed metal strip stretched rapidly. The speed of the hammerhead was estimated to be 6 m/s. Finally, the hammerhead hit the concrete block. From this result, the kinetic energy of the hammering by the device was calculated using Equation (4.3).

$$KE = \frac{1}{2}mv^2 \tag{4.3}$$

where the hammer mass m is 0.0017 kg, the impact speed v is 6 m/s, and the kinetic energy of hammering KE is 0.306 J. Ichikawa et al. [52] estimated that the hammering energy is approximately 0.3 J for human inspectors to find defects at a depth of approximately 100 mm from the surface. The calculated KE indicates that the developed device generates the same energy as the hammering of human inspectors.

The constancy of the hammering pulse magnitude was evaluated in 10 impact results, measured with a 16-kHz sampling rate for a loadcell set at the hitting point. The developed hammering device generated 1-Hz hammering. The impulse force was observed when the hammerhead contacted the loadcell, as shown in Figure 4-5 (left). The developed hammering device generated a constant force with a mean impulse of 215.9 N and a standard deviation of ±19.97 N. The developed hammering device realized a continuous impulse every second with a distribution of less than ±10%. To confirm the influence of the small force observed after the hitting impulse, the raw sound data of one hammering are shown in Figure 4-5 (right). The sound was not influenced by the small peak after the hammering impulse. This peak caused the hammerhead to move while contacting the loadcell when the metal strip stretched after hammering.

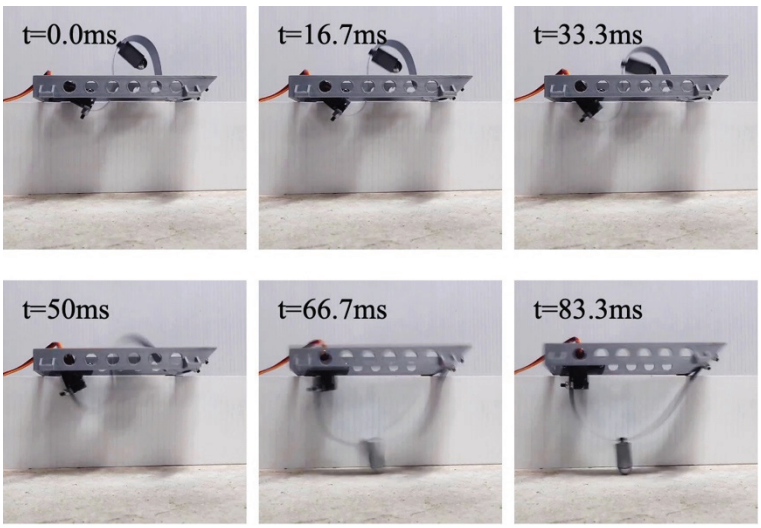

Figure 4-4 Hammering sequence by the developed device (60 fps).

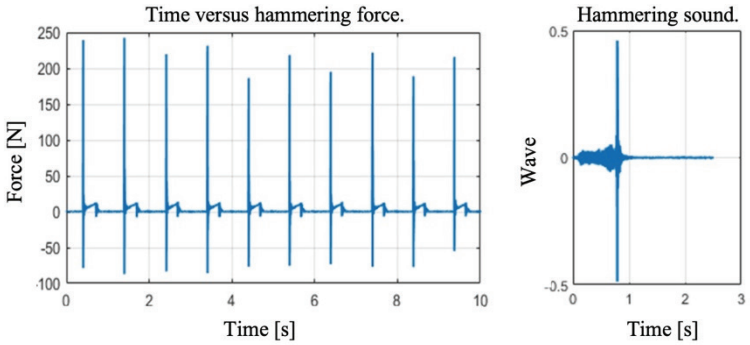

Figure 4-5 Hammering force and hammering sound.

4.2.2 Development of a Propeller-type Climbing Robot for Inspection

Development of Robot

Figure 4-6 shows the developed hammering inspection robot. The frame of the robot is made of carbon to reduce weight. Other essential components are made of 3D-printed parts made with PLA. Four DJI E310 2312 motors were used for propeller rotors, and Pololu 1000:1 HPCB 12-V geared DC motors were used to drive the wheels. For changing the direction of the robot, two steering wheels with two TowerPro SG90 servo motors were installed to turn on the surface. The length and width for both were 430 mm, and the height was 180 mm. The weight of the robot, including the hammering device and a Li-po battery (11.1 V, 1800 mAh), was 1.17 kg.

Figure 4-7 shows a robot using the proposed method to maintain a stable attitude on a structure. To ensure that the hammer hits the structure with enough power, the hammerhead was placed approximately 5 mm on the building side. A RODE Wireless GO Bluetooth microphone was installed near the hammering point under the robot. In the parameters of the developed robot, $F_{p\text{-}upper}$ and $F_{p\text{-}lower}$ were 11.76 N each, h_{COG} was 50 mm, l_{COG} was 105 mm, and l_p was 50 mm. The friction coefficient between wheels and concrete was approximately 0.72, and F_i, the average impact force per unit time calculated from Figure 4-5, was 2.48 N. The design satisfied the stability conditions of the propeller-type climbing inspection robot.

Fundamental Experiment

In the fundamental experiment, the developed robot climbed a vertical surface while hitting a structure. It was confirmed that the design of the proposed climbing robot realized the necessary movement for hammering inspection. The robot moved upward from the bottom part of the wall of the concrete structure. The robot moved up the experimental wall stably, and the mounted hammer hit the surface correctly. For a quantitative evaluation, a similar experiment was performed five times. When the robot climbed down 50 cm while hammering on a wall, the average position error was 3.7 mm, and the angular error was 0.6° per hammering hit. The diameter of the hammerhead was 10 mm, and the error within that range was acceptable. These errors resulted from a slight imbalance of the center of gravity of the robot to the left and right sides.

The developed robot had a speed of 4.4 m/min and a 10-min continuous operating time. The operating time depends on the battery size, but the robot in this study could also operate with a power cable from an external power source. Therefore, the robot realized a longer operation time within the range the cable reached. However, the weight of the cable must be considered under stable conditions in further research.

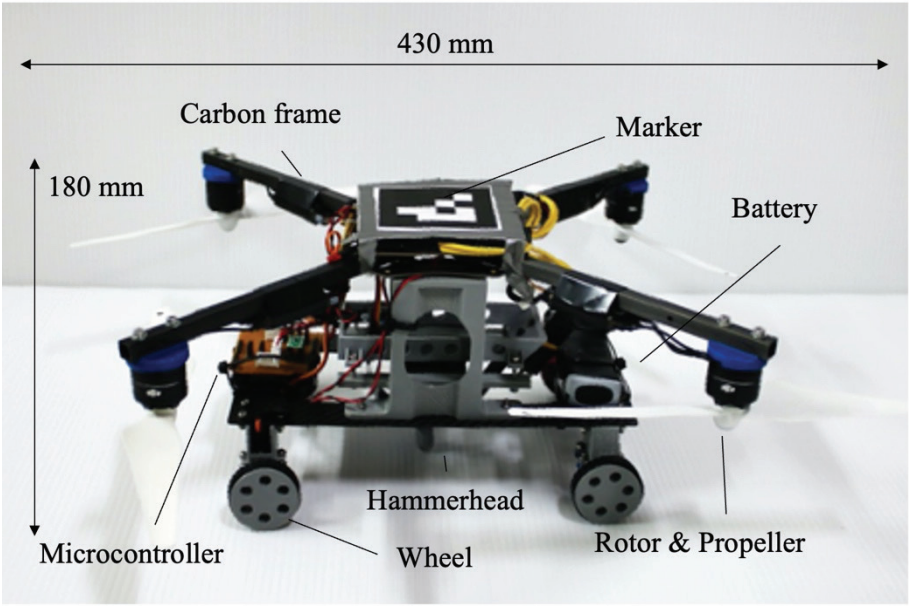

Figure 4-6 Developed hammering inspection robot.

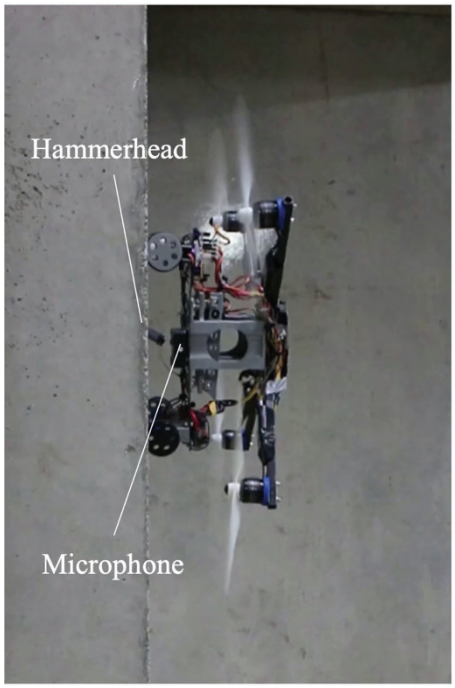

Figure 4-7 Developed hammering inspection robot on a wall.

4.2.3 Measurement of Hammering Position and Sound

The system records the hammering sound and the position in which the hammering was made. Here, the process of detecting the timing and position of the hammering is described. First, the estimation method of the timing of the hammering is described. The raw sound recorded by the microphone included intense wind noises from the propellers. Because of these wind noises, it was difficult to determine when the hammering occurred. Therefore, a high-pass filter with a 10-kHz cutoff frequency was used for noise removal. When the amplitude of the signal with noise removed exceeded a certain threshold, the system detected that hammering occurred. The original and denoised signals from the five hammerings are shown in Figure 4-8. A computer and a camera were prepared on the ground side. The video was captured by a camera on the ground, and the sound was recorded from a microphone mounted on the robot. The video and sounds were synchronized. Augmented reality (AR) markers [82] [83] were attached to the top of the robot to find its position on the structure surface. The robot position was calculated from the captured images using an AR marker. Figure 4-9 shows the estimated path of the robot with a white line and the hammering points estimated from the recording sound using a filter and threshold by a white dot. The yellow and blue dashed line represents the direction of the robot when moving forward and backward, respectively.

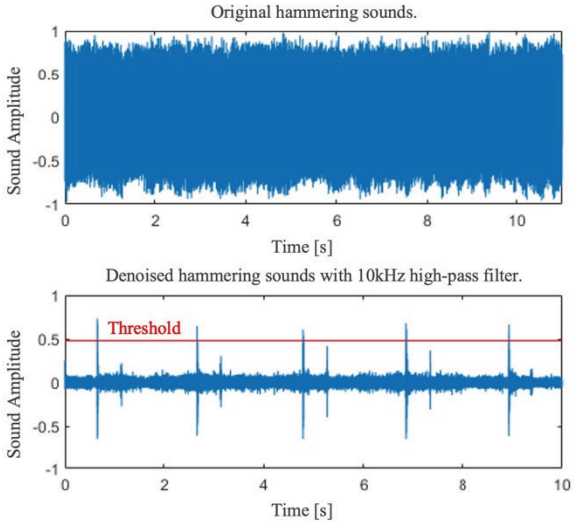

Figure 4-8 Recorded hammering sounds.

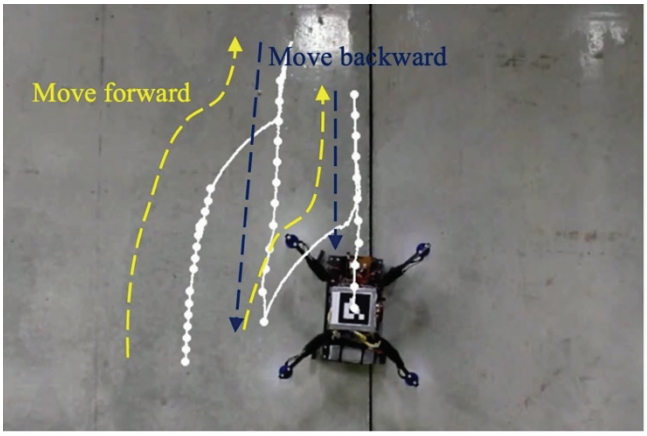

Figure 4-9 Estimated robot path and hammering points on a wall.

4.2.4 Acoustic Analysis

To perform a hammering inspection using a propeller-type climbing robot, the acoustic analysis must be designed to work under a high wind noise from the propellers. In previous studies, Ye et al. [84] proposed a machine-learning evaluation, Hagiwara et al. [85] proposed a statistical analysis, Kasahara et al. [86] proposed an active weak supervised analysis, and Shih et al. [87] and Fukumura et al. [88] proposed deep learning because sound characteristics change depending on the environment. Figure 4-10 and Figure 4-11 show the short-time Fourier transform (STFT) results for clear and defect sounds without and with noise, respectively. The hammering sounds were recorded on a clear area and a defect area with a sampling rate of 48 kHz using the developed system. The hammering occurred at 130 ms. The clear sound peaked around 2.5 kHz, while the defect sound peaked around 5–6 kHz. However, it is difficult to distinguish those characteristics from hammer sounds containing propeller noises. A simple two-class classifier was used to separate clear and defect sounds with a fully connected layer-based classification provided by the MATLAB deep-learning toolbox [89]. The timing of the hammering was determined by the method introduced in Section 4.2.1. To avoid losing features of the hammering characteristics, a raw sound file was used for creating a sound dataset. At the estimated hammering timing, the raw sound file was cut into single hammering sound data with a duration of 0.5 s, in which 25% were before and 75% were after the peak threshold was crossed. A total of 120 hammering sounds (60 clear and 60 defect) containing wind noises were collected for training the classifier. All sounds were collected from the surface of the Test 1 concrete in Section 4.2.5. The final model could classify the training dataset with 100% accuracy. The corrected sounds from the following experiment were used for validation, and the classifier model that achieved 100% accuracy on the training data was selected for validation.

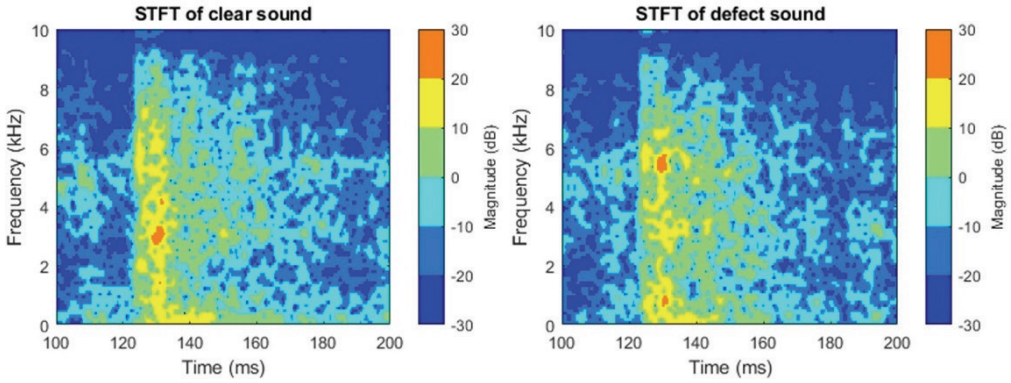

Figure 4-10 STFT of hammering sounds without noises.

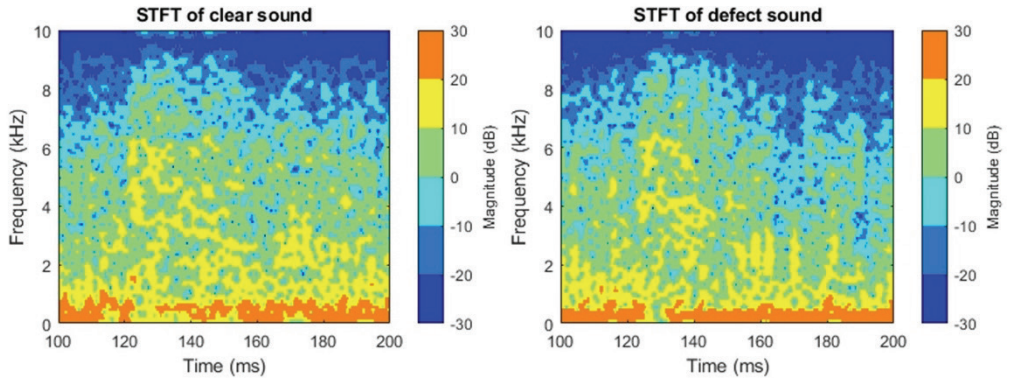

Figure 4-11 STFT of hammering sounds without noises from propeller-type climbing robot.

4.3 Experiment and Result

4.3.1 Experimental Setting

The experiment was conducted on two reinforced concrete structures (Tests 1 and 2) by using the developed robot to determine the accuracy of the inspection (see Figure 4-12 and Figure 4-12). Test 1 had an iron stage, three concrete walls, and a concrete ceiling. The height of the structure, including the stage, was 1980 mm, the width was 2280 mm, and the thickness of the concrete wall was 150 mm. A 200-mm square plastic plate was embedded 30 mm deep inside the concrete to simulate internal defects. The plastic plate was placed 900 mm from the left side and 1080 mm from the top of the structure. Test 2 also employed reinforced concrete with a height of 1680 mm, a width of 780 mm, and a depth of 150 mm. Artificial peeling was created using pipes filled with expansion agents [40]. In Test 2, a professional inspector performed a hammer test and marked the defect area (red area) that would be the correct answer for reference. The target areas where the data were collected are shown in the blue area.

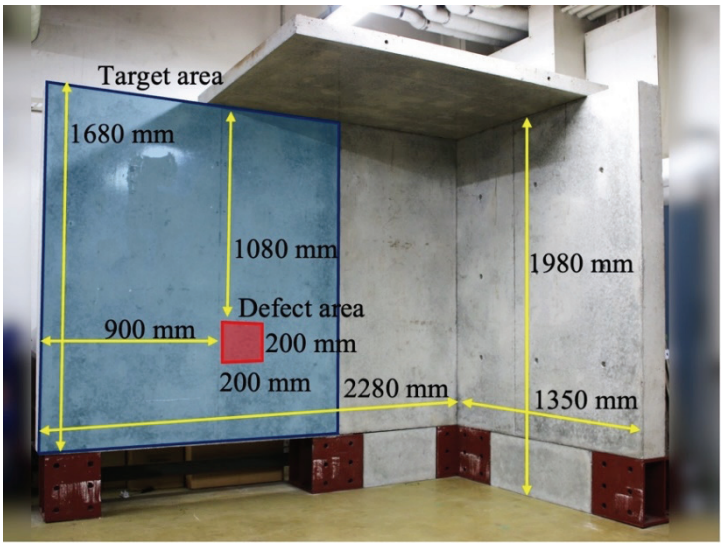

Figure 4-12 Test concrete structure 1.

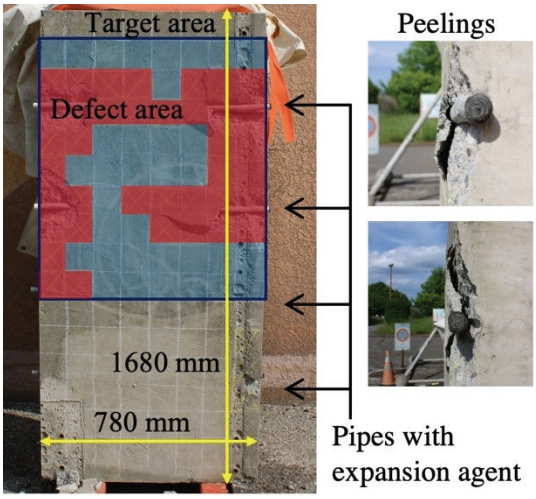

Figure 4-13 Test concrete structure 2.

4.3.2 Experimental Results

The developed robot moved on a wall surface and recorded the hammering sound made by the hammering device installed on the robot. The recorded sound was classified as clear or defect. The results are plotted in Figure 4-14, with red circles as defects and green circles as clears. In Test 1, the number of hammerings was 57, and six hammerings were when the AR marker overlapped the defect area. The labeled numbers indicate the order in which the experiments were performed. Table 4-1 shows the results of the classifier used in this study and the classification results of examining the peak frequency using spectral analysis for comparison.

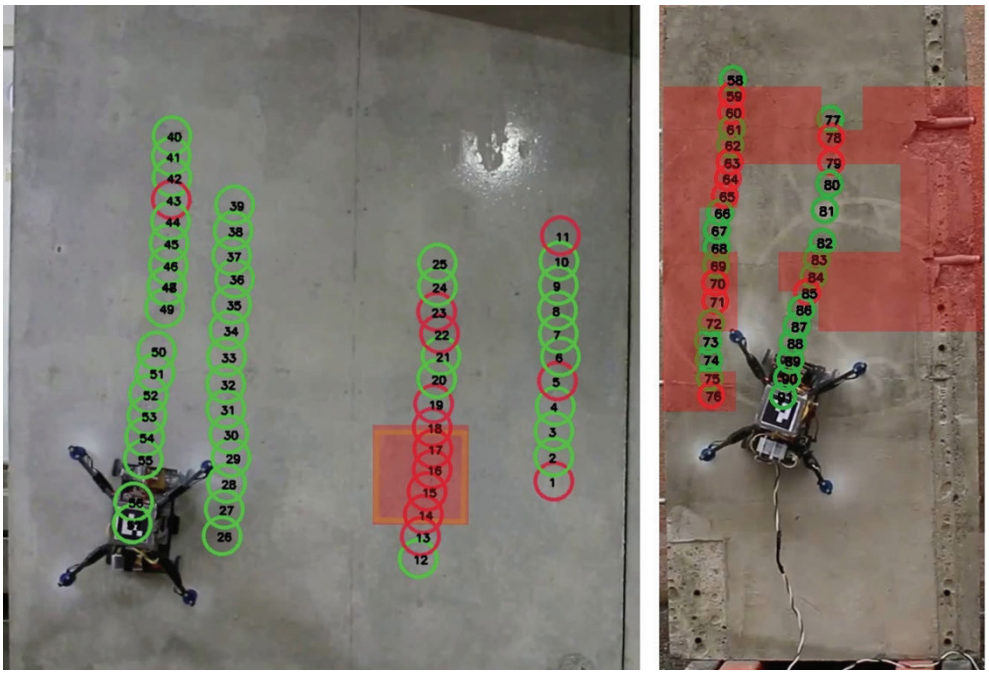

Figure 4-14 Hammering inspection results (left: Test 1, right: Test 2).

Table 4-1 Hammering sound classification results.

	Spectral Analysis			**Proposed**		
	Test 1	**Test 2**	**Total**	**Test 1**	**Test 2**	**Total**
Total Hits	57	36	93	57	36	93
True Positive	0	0	0	6	12	18
False Positive	0	0	0	7	2	9
True Negative	51	16	67	44	14	58
False Negative	6	20	26	0	8	8
Accuracy [%]	89.5	55.6	72.0	87.7	72.2	81.7
Recall	0.0	0.0	0.0	1.0	0.6	0.69
Precision	-	-	-	0.46	0.86	0.67

4.4 Discussion

A propeller-type climbing robot equipped with a hammer device using a snap motor was developed. It can keep a constant distance from the wall and hit the wall surface with a constant force. The classifier distinguished the recorded hammering sounds as clear or defect sounds. Inspection experiments on actual concrete structures in the presence of wind noise showed that the accuracy in detecting defects inside concrete was 81.7%.

The use of UAVs or mobile robots causes noise in sound data and makes it difficult to determine the characteristics of a hammering sound. With spectrum analysis, it is difficult to find peak values, and all hammering sounds were predicted to be clear. However, the proposed method had an overall accuracy of 81.7%, and the recall and precision were 0.69 and 0.67, respectively. The recall from Test 1 concrete was 1.0, so the inspection result did not have undetected defects. Moreover, data recorded from Test 1 were used for training and validation, so Test 2 was an unknown concrete for the trained classifier. However, the result shows an accuracy of 72.2% with a recall of 0.69, even in the presence of strong noises.

To put this system to practical use, the robot should hit the surrounding area with high density once a hitting sound is predicted as a defect. For example, the hammering sounds of Nos. 13–19 were predicted as defects. The reality for Nos. 13 to 19 was also a defect. However, Nos. 5 and 45 were predicted as a defect. The surroundings were predicted to be clear, and the reality was also clear. The developed robot collected sound data by hammering the wall continuously while moving on the surface. Therefore, the proposed system showed potential for use in actual hammering inspection. Furthermore, the accuracy of the inspection was analyzed. In previous studies, the inspection accuracy for concrete hammering by the climbing robot was not reported.

Chapter 5 Application 2: Grass Cutting on Steep Slope

5.1 Overview of Grass-Cutting Robot

Grass cutting on steep slopes is dangerous during agricultural activity in hilly and mountainous areas. Therefore, an attempt was made to perform grass-cutting tasks on steep slopes using a robot. In developing the robot, four steering methods (two-wheel steering, skid steering, mecanum wheels, and four-wheel steering) were compared to find a suitable method for the propeller-type climbing robot to perform area coverage tasks on inclined surfaces.

5.1.1 Introduction of Proposed Grass-cutting Robot for Slopes

In agriculture in hilly and mountainous areas, grass-cutting work is performed on slopes of up to 60°, causing a burden for farmers. In Chapters 3 and 4, a quadcopter-based propeller-type climbing robot was proposed. However, using a quadcopter requires a wider frame so that the propellers do not contact each other. For this reason, the propellers stick out from the side of the robot body. Therefore, there is a high possibility that the propellers will contact the ground, grass, and other objects. A propeller-type climbing robot, as shown in Figure 5-1, was proposed to ensure safety. In addition, related research on climbing robots has not examined methods to move freely on inclined surfaces. Therefore, considering the stability when the robot changes direction, the four methods were compared, and the optimal method for a grass-cutting robot was adopted.

Figure 5-1 Computer-aided design of the proposed grass-cutting robot.

5.1.2 Stability of Grass-Cutting Robot on Slopes

A force diagram of the proposed robot is shown in Figure 5-2. The stable conditions are modified to fit the design of the proposed robot, which has two propellers at the center. Here, g is the gravity acceleration, μ is the friction coefficient, m is the mass of the robot, θ is the slope inclination angle, F_p is the thrust force, ϕ is the thrust tilted angle, h_{COG} and h_p are the heights of the center of gravity and propeller, respectively, and l_{COG} is the length between the wheel and the center of gravity. For no slip to occur for the robot on a slope with angle θ, the robot must satisfy the following condition:

$$\mu\left(mg\cos\theta + F_p\cos\phi\right) \geq mg\sin\theta - F_p\sin\phi \tag{5.1}$$

Equation (5.1) is the same condition as Equation (3.5). The proposed robot falls when the wheels on the upper side of the slope leave the ground. Therefore, the proposed robot must satisfy

$$\frac{mg}{L}\left(l_{COG}\cos\theta - h_{COG}\sin\theta\right) + \frac{F_p}{L}\left(l_{COG}\cos\phi + h_p\sin\phi\right) \geq 0 \tag{5.2}$$

In this study, $N_{upper\text{-}right}$, $N_{upper\text{-}left}$, $N_{lower\text{-}right}$, and $N_{lower\text{-}left}$ are the normal forces acting on the upper-right, upper-left, lower-right, and lower-left wheels, respectively. When the robot is facing in the vertical direction on a slope, $N_{upper\text{-}right}$ is the same as $N_{upper\text{-}left}$, and $N_{lower\text{-}right}$ is the same as $N_{lower\text{-}left}$. The normal forces are written as

$$N_{upper-right} = N_{upper-left} = \frac{1}{2}\left\{\frac{mg}{L}\left(l_{COG}\cos\theta - h_{COG}\sin\theta\right) + \frac{F_p}{L}\left(l_{COG}\cos\phi + h_p\sin\phi\right)\right\} \tag{5.3}$$

$$N_{lower-right} = N_{lower-left} = \frac{1}{2}\left\{\frac{mg}{L}\left(l_{COG}\cos\theta + h_{COG}\sin\theta\right) + \frac{F_p}{L}\left(l_{COG}\cos\phi - h_p\sin\phi\right)\right\} \tag{5.4}$$

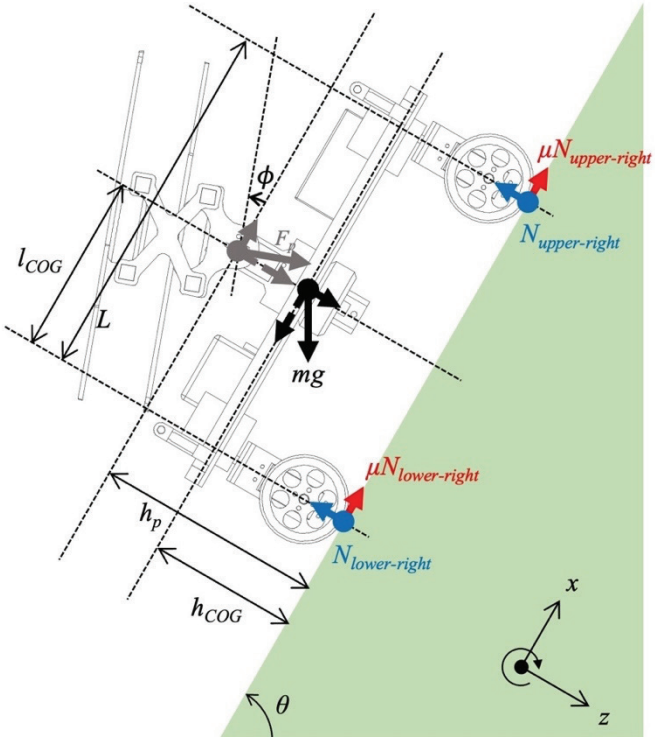

Figure 5-2 Force diagram of the proposed grass-cutting robot.

5.2 Design and Fabrication

5.2.1 Steering Methods of Grass-Cutting Robot

Four steering methods were examined to select the optimal steering method for grass-cutting tasks on steep slopes. Figure 5-3(a)-(d) show the steering methods used. The black arrow represents the direction of each wheel, and the red arrow represents the moving direction of the robot as a result of wheel rotation. (a) Two-wheel steering is a common method for controlling wheeled vehicles, such as automobiles and buggies. (b) Skid steering is used for robots with tracked wheels. When turning with skid steering, the robot rotates one side of the wheels forward and the other side of the wheel backward. (c) The mecanum wheel enables the robot to move freely by independently changing the rotation direction of each wheel. (d) Four-wheel steering uses four drive wheels connected to the steering actuators. When the robot with four-wheel steering changes direction, the steering actuator is controlled to rotate 90°.

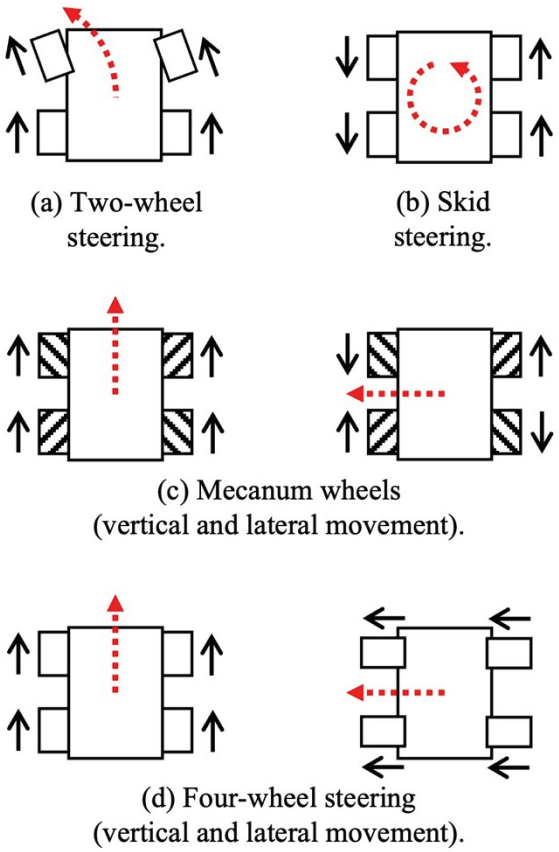

Figure 5-3 Four types of steering method.

Through simulation, the optimal motion type of the robot when cutting grass was confirmed. The steering methods on the inclined surface were classified into a movement method that cannot make a 90° turn at one position and a movement method that can make a 90° turn. Figure 5-4 shows a result of the grass-cutting simulation, assuming that the robot starts its work from the bottom and climbs the slope while cutting grass in the target area, shown as inside the yellow dotted line. In case 1, shown in the yellow masked area, the grass in the corner of the target area cannot be cut in a single movement of the robot. Therefore, the robot must return to the area where the grass cutting has been finished to cut the leftover grass. In case 2, the robot climbs a slope, makes a 90° turn, and moves sideways directly. Thus, the robot can perform grass cutting in the corners of the target area efficiently and effectively. In this study, the robot that can make a 90° turn is controlled to move left and right on the surface instead of up and down against gravity from the viewpoint of mechanical energy.

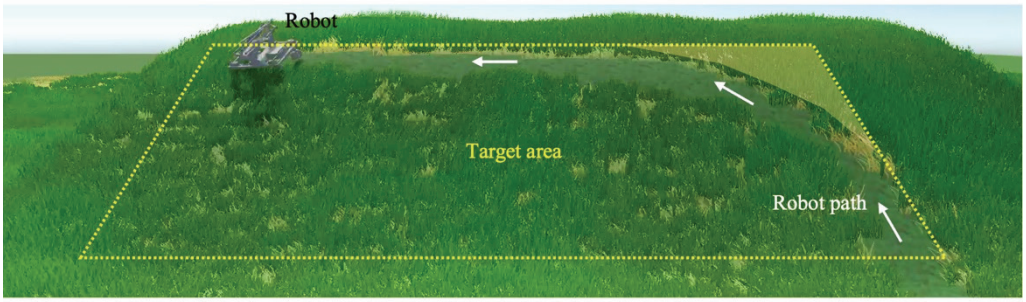

(a) Case 1: Grass cutting by a robot with two-wheel steering.

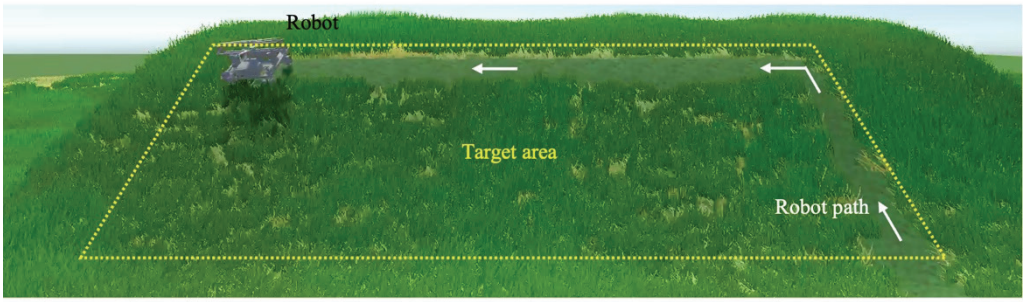

(b) Case 2: Grass cutting by a robot with four-wheel steering.

Figure 5-4 Result of grass-cutting simulation.

5.2.2 Development of Grass-Cutting Robot

Developed Robot

Here, details of the developed robot(Figure 5-5) are described. A carbon pipe was used for the robot frame to lighten the weight. Four FEETECH FT5325M servo motors were attached as steering actuators to a robot base made of acrylic boards. Four FEETECH FB5311M-360 continuous rotation servo motors were used for wheels. For the propeller mechanism, two TAROT TL68P02 brushless rotors with HobbyWing Skywalker 60A ESCs were used to rotate the propellers. Two FEETECH FT5325M servo motors connected the robot base and propeller mechanism on a one-degree-of-freedom axis. A nylon cord was used for the grass-cutting module because nylon cords are safer and lighter than a metal blade (Figure 5-6). The length of the robot was 305 mm, the width was 290 mm, and the height was 242 mm. The robot weight was 2.9 kg, including a LiPo battery (6500 mAh, 14.2 V). The robot produced a maximum thrust force of 20 N. By substituting the actual parameters, mg = 28.4 N, θ = 60°, F_p = 20 N, ϕ = 20°, L = 250 mm, l_{COG} = 125 mm, h_{COG} = 100 mm, h_p = 150 mm, μ_{rubber} = 0.92 on the rubber surface, and μ_{grass} = 1.25 on the grass, into Equations (5.1) and (5.2), the two conditions for stability on an inclined surface at an inclination angle of 60° were satisfied. The robot must perform grass cutting on a slope up to 60°, and the stability models show that the proposed robot can work on slopes with an angle of 60°.

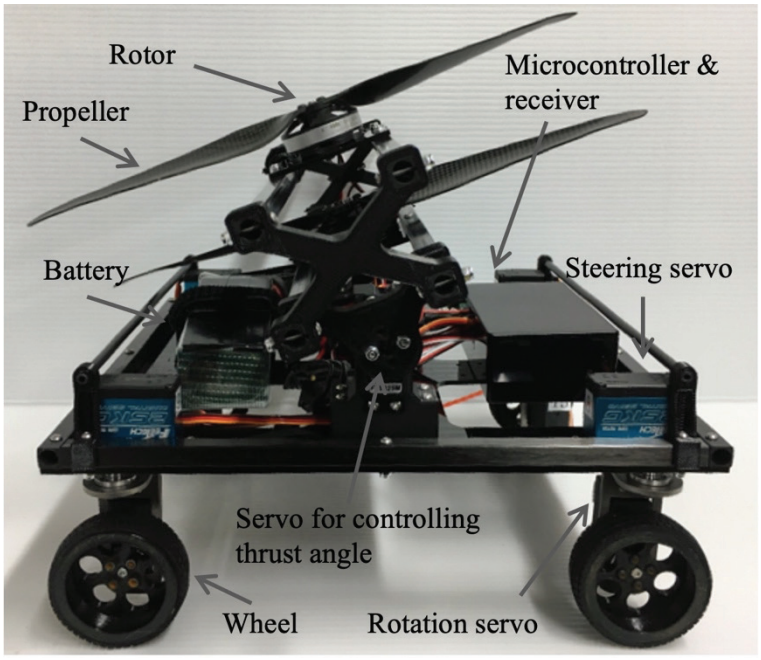

Figure 5-5 Developed grass-cutting robot.

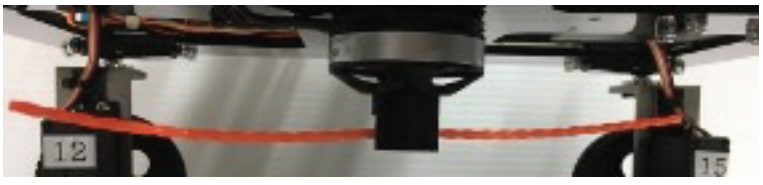

Figure 5-6 Grass cutter with nylon cord.

Fundamental Experiment

First, the fundamental experiment was conducted to test the basic ability of the robot. As shown in Figure 5-7(a), a normal wheel was used initially, but the robot could not overcome grassy terrain because the wheel was buried in the grass. To improve the movement on grass, spikes were added to the wheel, as shown in Figure 5-7(b).

The fundamental experiment investigated how straight the robot could traverse sloped grassy terrain. Iwano et al. [13] proposed an experiment to measure the slipped distance when a robot moves on a linear trajectory along a 45° inclined slope. The robot developed by Iwano et al. [13] slipped down 180 mm to the downside direction while traveling a distance of 2.5 m along the slope. In this study, the same experiment was conducted on grassy terrain where the slope angle was a maximum of 45°. The results of the experiment are shown in Figure 5-8. Because the test was conducted in a natural environment, the inclination angle of the tested slope ranged from 42° to 45°. Without any difficulty, the developed robot traveled 2.5 m with no slip, even in areas where the terrain was slightly curved and the inclination angle changed.

(a) Normal wheel. (b) Spiked wheel.

Figure 5-7 Normal and spiked wheels.

Figure 5-8 Straight lateral movement on grass terrain with 45° inclination.

5.2.3 Steering Method Selection

To select the optimal steering method from the four steering methods described above, an experiment was conducted. For the experimental surface, a 1.8m × 0.9 m wooden board covered with a rubber sheet was prepared and inclined 60° (Figure 5-9). The robot was controlled to climb 0.6 m from the ground, turn 90° to the left, and make a straight move along the experimental slope until the robot moved 1.0 m to the left. Figure 5-10 shows the movement of the robot during each steering method, and Figure 5-11 plots the path of the robot for each steering method.

The method with the mecanum wheel could not climb the slope at first because the small spinning wheels of the mecanum wheel slipped when the robot attempted to climb. In the method with skid steering, the robot could climb the slope, but, when it tried to turn, it slipped down the slope. In two-wheel steering, the robot could reach the target point but could not easily approach the corner, as shown in the simulation in Section 5.2.1. The four-wheel steering robot moved on slopes without deviating from the target path. Although there was a slight occurrence of slips, the effect of slips close to negligible in the grass-cutting operation, as confirmed by the fundamental experiment in Section 5.2.2, because the friction coefficient is larger in grassy terrain than on rubber ($\mu_{grass} = 1.25$, $\mu_{rubber} = 0.92$).

The results demonstrated that using four-wheel steering is a suitable method for a propeller-type climbing robot for a grass-cutting task on steep slopes in hilly and mountainous areas. Therefore, the following experiment was conducted using four-wheel steering.

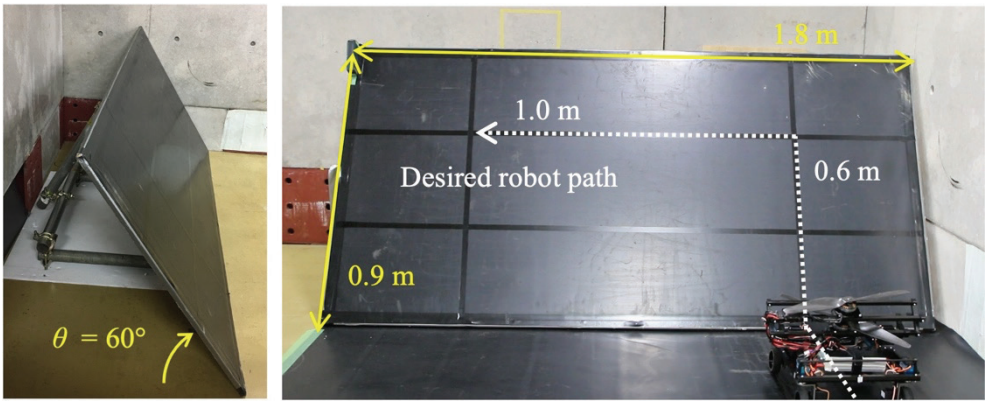

Figure 5-9 Experimental setting for steering method selection.

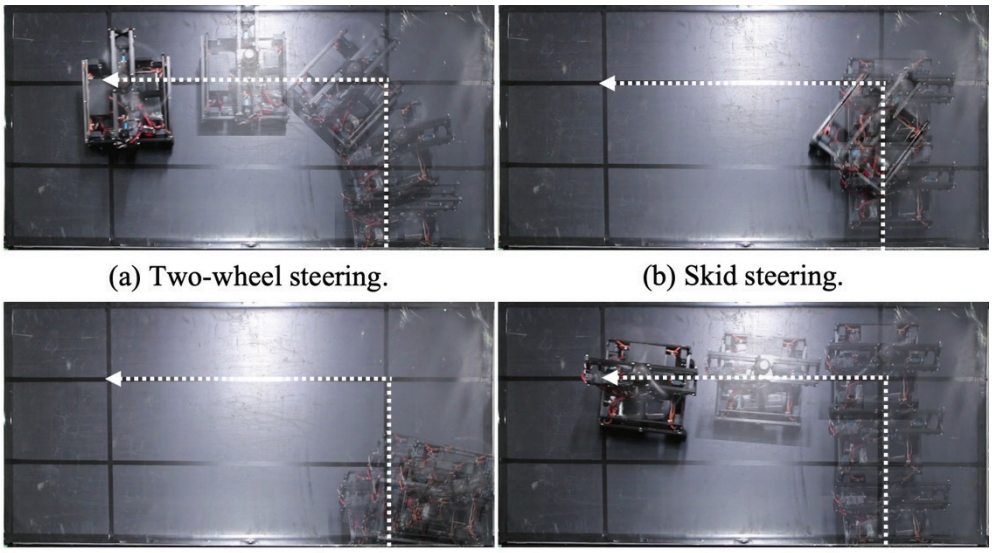

(a) Two-wheel steering. (b) Skid steering.

(c) Mecanum wheels. (d) Four-wheel steering.

Figure 5-10 Steering comparison on rubber slope with 60° inclination.

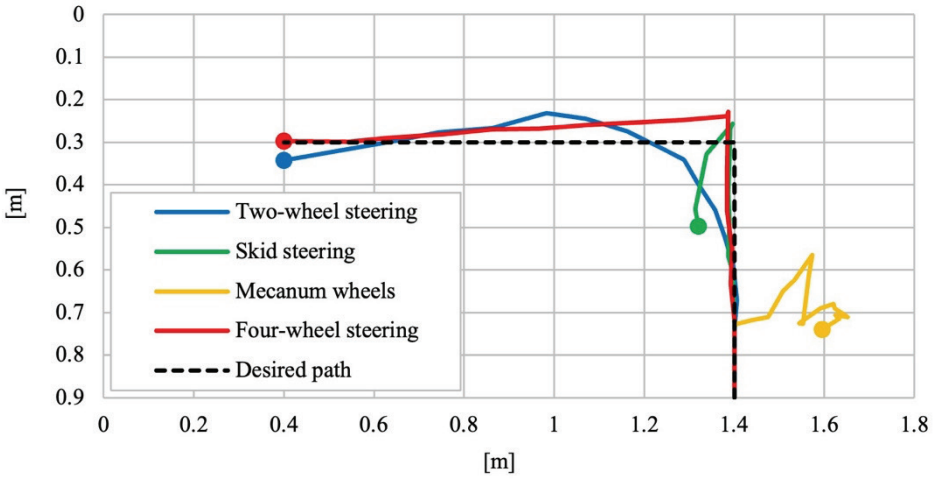

Figure 5-11 Path of the robot during the steering experiment.

5.2.4 Area Coverage Experiment

Grass cutting is an area coverage task because the robot must pass through the target area without omission, not just move to a destination. In Section 5.2.3, straight movement of the robot on an inclined surface was examined. Therefore, the area coverage experiment was performed to investigate how much coverage can be achieved on steep slopes. Only a few previous studies have reported coverage when moving on slopes. Veerajagadheswar et al. [27] conducted an experiment to measure the coverage percentage on 20° and 30° slopes with their robots and reported achieving more than 98% and 95.07% of the total area coverage, respectively. In this study, experiments were conducted to verify the area coverage capability under the same experimental setting [27], just changing the angle.

First, area coverage was measured on a slope with a rubber surface. A slope with L = 1.7 m and $W = L/2$ was prepared, as shown in Figure 5-12. The robot was placed at the bottom left as the initial position. The coverage area was calculated based on video recordings. Figure 5-13 shows the coverage process (green area) of the robot at different time points. To enable the developed robot to achieve stable movement when climbing and moving laterally, the coverage area percentage on the rubber surface with an inclination angle of 60° was 99.95%. The proposed robot significantly improved the inclination angles with a high coverage area on surfaces.

Second, the coverage area was measured on grassy slopes in hilly and mountainous areas. The target area size was the same as in the previous experiment. The robot was controlled to move around the area. Anchors were embedded in the grass to show the target area. The experimental setup is shown in Figure 5-14. Figure 5-15 shows the coverage process (green area) of the robot at different time points. The target area in which the experiment was conducted had an inclination angle ranging from 45° to 50°. The coverage area percentage was 98.45% on grassy terrain. The robot could not cover the area around the bottom of the target area because the robot was controlled to avoid edges where the inclination angle changed from 0° to 49°.

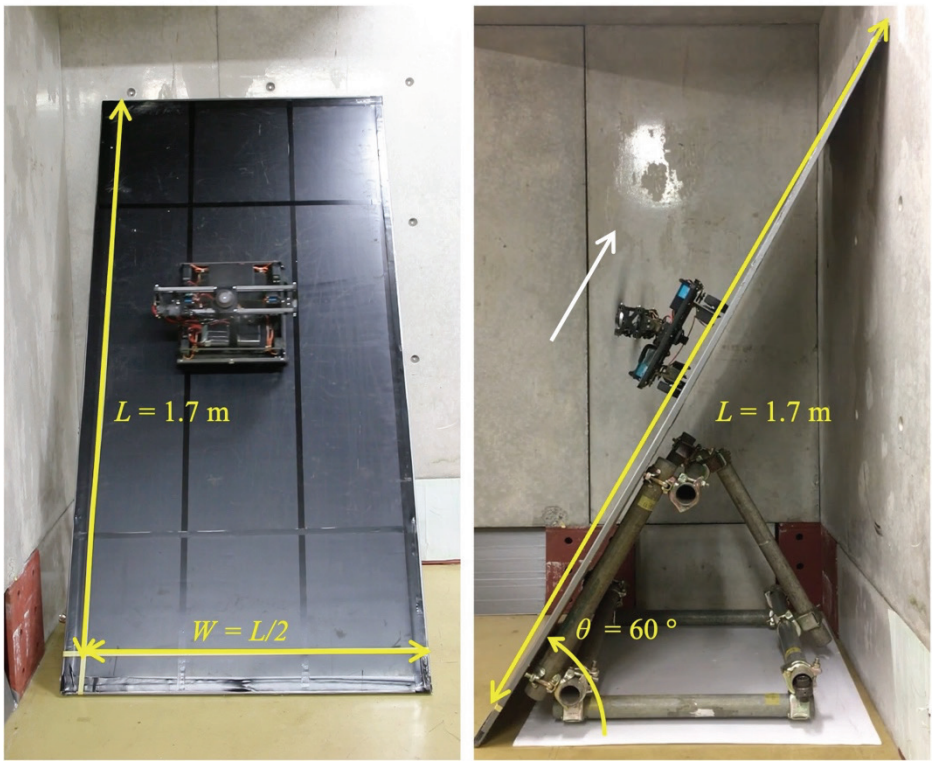

Figure 5-12 Experimental setting of area coverage experiment (rubber).

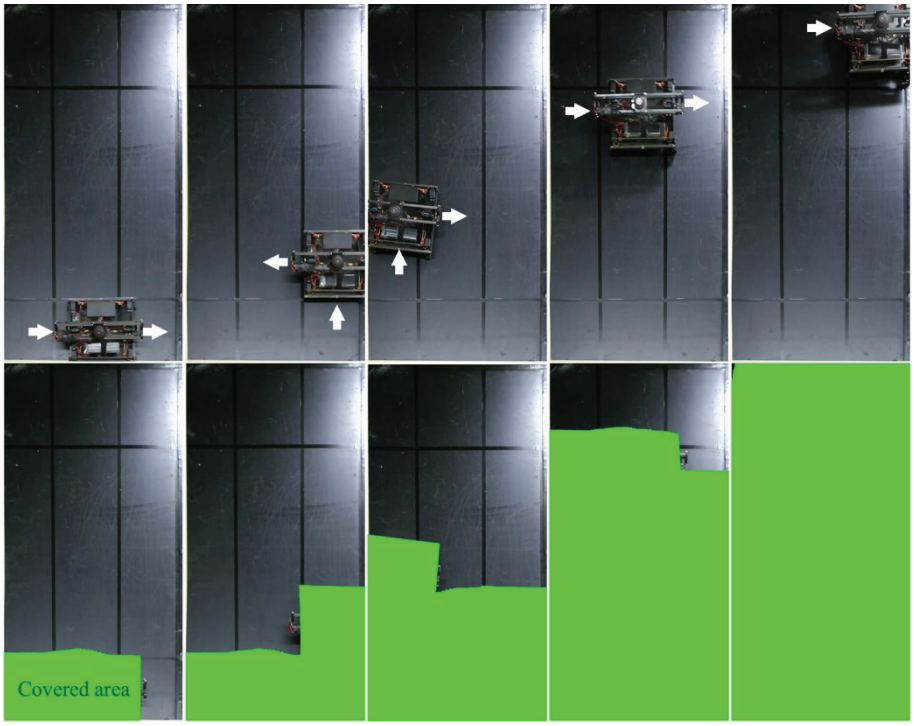

Figure 5-13 Experimental result of area coverage experiment (rubber).

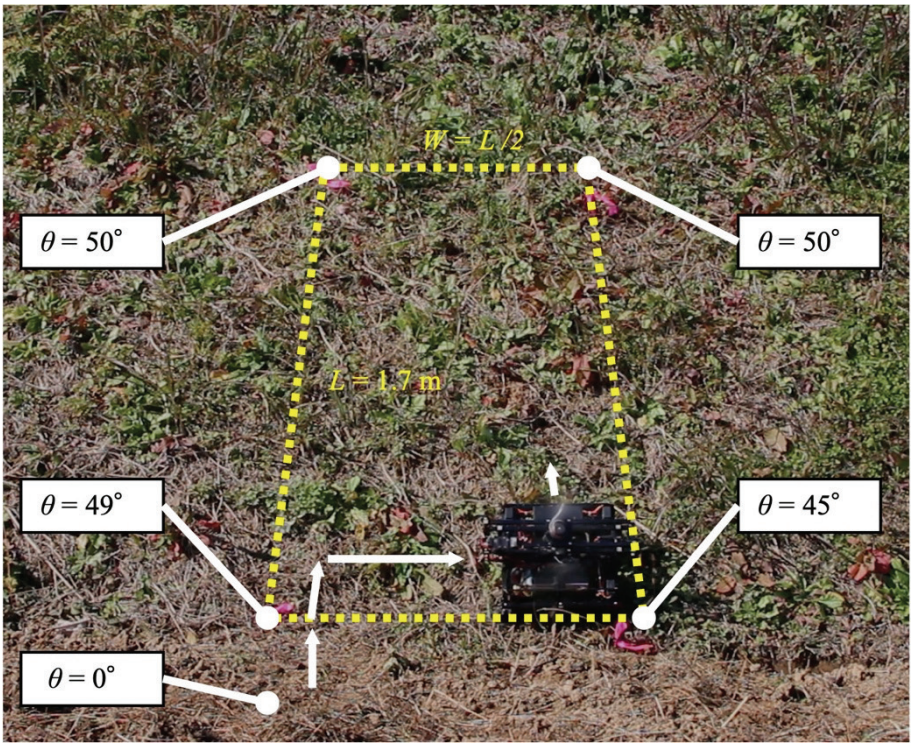

Figure 5-14 Experimental setting of area coverage experiment (grass).

Figure 5-15 Experimental result of area coverage experiment (grass).

5.3 Experiment and Result

Finally, grass-cutting tasks by the developed robot were performed on slopes in hilly and mountainous areas. Figure 5-16 shows a grass-cutting experiment on a slope with an inclination of 33° to 44°, and 30-cm-tall grass was cut to approximately 5 cm. This experiment confirmed that the developed robot can cut grass properly with the nylon cord grass-cutting module. The nylon cord was selected for safety reasons because it can cut only soft materials, such as grass. Moreover, the nylon cord is lighter and has small inertia compared with a metal blade. Figure 5-17 shows that the robot can maintain a stable attitude, climb, and move along a slope with an angle of 60° without slips and falls. This slope had the maximum inclination angle in the experiments.

Figure 5-16 Grass cut by the nylon cord equipped on the robot.

Figure 5-17 Climbing on a 60° slope in a hilly and mountainous area.

Figure 5-18 and Figure 5-19 show grass cutting on slopes between cultivated land in hilly and mountainous areas. As shown in Figure 5-18, the robot started from the top of the slope, moved to the left side, climbed down the slope a little, then moved to the right side. The robot repeated this sequence of movements while cutting grass. The robot moved from the upper left to the lower right side on the slope, as shown in Figure 5-19. The range of inclination was from 18° to 55°.

Figure 5-18 Grass cutting on a slope with an inclination angle of 41° to 55°.

Figure 5-19 Grass cutting on a slope with an inclination angle of 18° to 40°.

5.4 Discussion

Grass cutting in hilly and mountainous areas is a complex operation performed on uneven terrain with a large inclination angle. Accidents have been reported when farmers cut grass on steep slopes at angles up to 60°. In this study, a novel grass-cutting robot was developed. The robot was designed based on stable conditions. The propeller-type climbing robot with four-wheel steering was proposed to realize stable movement on steep slopes while cutting grass.

Four steering methods were compared in the development process. For robots performing area coverage tasks, a 90° turn is important because it reduces the uncovered area around the corner of the target area. As a result of the comparison, four-wheel steering was selected. The robot was compared with previous studies in terms of the straightness of motion and the coverage area percentage. The experiment resulted in coverage area percentages of 99.95% and 98.45% on a rubber surface and grassy terrain slopes, respectively. Finally, grass-cutting experiments were performed on different slopes, and the grass was cut as expected. The speed of the robot was approximately 16 cm/s. The battery had 23 min of power with medium thrust. Thus, the robot can cover an area of 66 m^2 in one operation.

In future work, the automation of grass cutting by the proposed robot should be considered for practical application of the robot. Although the robot has a significant advantage in inclination angle, the autonomous navigation, grass-cutting accuracy, and working capacity should be compared with commercial products.

Chapter 6 General Conclusions

6.1 Conclusion

Mobile robots to perform tasks were studied. The purpose was to propose a new stabilization method and optimal movement method for mobile robots that can work on inclined surfaces. The proposed method enables the robot to work in more-complex environments. The proposed propeller-type climbing robot used thrust force to push the robot body against the surface to stabilize its attitude and locomotion on inclined surfaces. The applicability of a propeller-type climbing robot to realize tasks was examined. This study focused on hammering inspection and grass cutting as examples of work conducted on inclined surfaces. Through the development of applications for hammering inspection and grass cutting, the theory of propeller-type climbing robots that work on inclined surfaces was established. In Section 1.3, three research questions were clarified. The following conclusions were drawn for these three issues.

Can a propeller-type climbing robot realize a stable attitude for executing tasks on inclined surfaces?

To answer this question, the stable condition of the proposed propeller-type climbing robot was formulated in Chapter 3. Working on inclined surfaces requires mobile robots to achieve a stable attitude and movement by overcoming the problem of slips and falls. In Chapter 1, the conventional approach to achieving stable movement was described. Propeller-type climbing robots have a high potential to be applied to work robots because the limitation of the surface material and condition is relatively small. To arrive at the optimal design of propeller-type climbing robots, simulation of a propeller-type climbing robot was conducted from the viewpoint of magnitude and direction of thrust force to avoid slips and falls while moving on inclined surfaces. The developed robot was equipped with four propellers that generated thrust force with an axis that controlled the direction of the thrust force. The lateral movement of robots on inclined surfaces was analyzed experimentally, whereas other studies have tended to focus on climbing ability. The experimental results demonstrated that a stable attitude and movement were achieved at an inclination angle of up to 90° when the magnitude and direction of the thrust force were controlled. Although the developed propeller-type climbing robots achieved a stable attitude on inclined surfaces, the robot must realize the actual task. The ability to perform tasks is essential for mobile robots to be adopted. Therefore, the implementation the proposed propeller-type climbing robot should be studied to show its effectiveness.

Is the stability of a propeller-type climbing robot influenced by interactions between the robot and the environment? If so, how should this interaction be managed?

When robots perform work, the work actuator attached to the robot interacts with the external environment. The influence on robot stability of the interaction between the robot actuator and environment was clarified in Chapter 4 through the development of a hammering inspection robot because the hammering actuator mounted on the robot must hit the surface while moving on a wall. It is necessary to consider the effect of this blow on the posture of the mobile robot. To perform a

hammering inspection, a propeller-type climbing robot with a lightweight hammering device, acoustic analysis that considers wind noises from propellers, and hammering positioning were implemented. The developed system had an 81.7% defect detection accuracy, whereas the hitting strength and number of successful strikes were considered in previous studies of hammering robots. In this study, the hammering force was included in the stability conditions of the robot. The impulse caused by the hammering does not significantly impact the attitude of the robot, so stable conditions were expressed with the average impact force per unit time. Furthermore, the classifier of defect sounds was trained by considering an environment heavily affected by wind noise from the propeller. An issue when implementing applications using a propeller-type climbing robot was analyzed because the aim of this study was to perform work on inclined surfaces. However, the steering method for propeller-type climbing robots has not been verified sufficiently. When a robot performs work on an inclined surface, the steering method significantly affects the work efficiency. There are two types of work robot: those that move to a target point and those that perform specific tasks on the entire target area on the surface. Examples of the work type in which robots perform specific tasks in the entire target area include inspection, cleaning, and grass cutting. Therefore, a steering experiment was conducted, as described in Chapter 5, to compare two-wheel steering, skid steering, mecanum wheels, and four-wheel steering for the locomotion of the propeller-type climbing robot.

Is the four-wheel steering method suitable for a propeller-type climbing robot that performs area coverage tasks on inclined surfaces?

The application adaptability of a propeller-type climbing robot on a vertical surface was demonstrated, as discussed in Chapter 4, by developing a hammering inspection robot. Propeller-type climbing robots are considered effective in implementing applications on steep slopes as well as on walls. Therefore, grass cutting on steep slopes with an inclination of up to 60° in hilly and mountainous areas was considered. A novel propeller-type climbing robot with two propellers at its center, four-wheel steering, and a nylon cord grass-cutting module was developed. The robot was optimally designed and evaluated in terms of steering method, straight lateral movement on steep slopes, climbing ability, and coverage area. It was confirmed that the robot could cover 98.45% of inclined grassy terrain with four-wheel steering. The robot could cut grass on various slopes with different inclination angles in hilly and mountainous areas.

A propeller-type climbing robot to perform work was proposed. The stability conditions on inclined surfaces were modeled, and the interaction between the actuator and the external environment when the robot performed tasks on inclined surfaces was considered. An experiment with various steering methods was designed to demonstrate the efficiency and effectiveness of the robot. Both the hammering inspection system and the grass-cutting system developed demonstrated the ability of robots to perform actual tasks.

6.2 Limitations

Limitation of Friction Coefficient

The proposed propeller-type climbing robot obtains a large friction force when the robot is pushed against a surface and obtains a large normal force. As discussed in Chapter 3, the magnitude and direction of thrust force were controlled according to the inclination angle of the surface. However, the required thrust force was determined by the friction coefficient and the inclination angle. Therefore, the friction coefficient is an important parameter, but it is difficult to measure in real time. The proposed robot cannot be applied on surfaces where the friction coefficient is difficult to measure in advance. On an inclined surface where the friction coefficient is unknown, the thrust force must be controlled with the lowest expected value of the friction coefficient to maintain a stable attitude. Therefore, it is necessary to estimate the friction coefficient of the ground from sensors to control the thrust forces. Higa et al. [90] estimated the relationship of forces applied to wheels and slips using a six-axis force sensor. Brandão et al. [91] proposed the prediction of friction coefficients from the vision of humanoid robots but not wheeled robots. However, in this study, friction coefficient estimation and slip avoidance were not used.

Limitation of Operation Time

The developed propeller-type climbing robot is driven by a battery. Therefore, there is a limitation in terms of operating time. The size of the battery determines the operating time. However, if the battery size is increased to extend the operating time, the weight of the robot increases, and the robot becomes unstable on inclined surfaces. While on the robot performs tasks, frequent battery changes are required when the operating time is short. Extending the operating time by using a wired power supply can replace the battery. Kiribayashi et al. [92] developed a tethered power UAV by controlling cable tension and direction with the developed device to reduce the influence of cable weight. However, the stability condition changes caused by the cable weight for a propeller-type climbing robot were not considered. Therefore, it is necessary to model stability conditions that include the influence of the power cable. Furthermore, the power consumption of rotors for propellers is large. For example, one rotor requires a current of more than 20 A. As a result, if the power cable becomes long, sufficient power cannot be supplied because of the loss from the electrical resistance of the power cable. Therefore, a method of sending power with high voltage and low current through a cable and a step-down converter on the robot providing a high current is conceivable. However, this method has not been implemented or evaluated.

Limitation of Developed Robots

As shown in Figure 3-11, the robot can realize a stable attitude with a minimum thrust force when the thrust tilted angle is 45°. The sum of $\cos\phi$ and $\sin\phi$ is maximized when ϕ is 45° so that the thrust force can be used most effectively. However, the developed robot could only realize ϕ in the range of −20° to 20° because a large thrust tilted angle requires propellers installed higher from the ground. Then, the center of gravity moves to a higher position, and stability against falls is reduced. The thrust force that the robot can output depends on the rotor and propeller sizes. Depending on the parts used in the robot, the possible thrust angle and center of gravity position can change. Therefore, it is necessary to redesign the robot according to the actual robot parts by comparing their specifications and weights.

In this study, a hammering inspection robot system was developed. In the process of structure maintenance, workers conduct further inspections, such as breaking surface concrete and checking the reinforcing steel inside concrete after finding defects in the hammering inspection. Moreover, repair is necessary after finding the defect. The currently developed robot cannot perform tasks requiring a heavy actuator with strong contact forces. The stability condition was tested, as described in Chapter 4. Such tasks can be realized if the thrust force is large. Further research on propeller-type climbing robots and their application is needed.

The experiments described in Chapter 5 confirmed that the grass-cutting robot could perform tasks on slopes in hilly and mountainous areas. However, some slopes are extremely uneven, with huge bumps and dents. Therefore, the wheels of the robot may not touch the ground properly. The stability of the propeller-type climbing robot relies on the friction force. Thus, the proposed method cannot be applied when the wheels cannot touch the ground. In addition, a characteristic of grass cutting is that the grass that has been cut remains as garbage. The wind from the propeller also blows the cut grass into the air during operation. These are not problems if grass is cut regularly. However, future development of grass-cutting robots on steep slopes should consider these issues and propose solutions.

6.3 Outlook

In this section, the prospects are explained based on the research results of the developed application. In this study, hammering inspection and grass cutting were robotized, but the tasks were not fully automated. For the inspection robot discussed in Chapter 4, the accuracy in detecting defects should be improved by detailed analysis of the hammering sound. In this study, the developed robot was only tested on a concrete wall. Further experiments on actual structures, including ceilings and curved surfaces, are expected. The grass-cutting robots must be able to move between target slopes in hilly and mountainous areas. The targeted areas between cultivated lands are not interconnected, so the robot must move from one terraced terrain to another. To realize fully automated grass-cutting robots, localization of the robot, such as using the Global Navigation Satellite System [93], should be implemented. To predict slips and falls in advance and realize a more stable attitude, a self-position estimation, such as using an inertial measurement unit [94], is required, so the robot must be equipped with sensors, such as cameras, to detect obstacles and determine the route of movement automatically

Finally, the developed propeller-type climbing robots should be brought to actual sites, and field studies should be conducted to improve the system while providing feedback. Through such measures, a robot that can play a wide range of societal roles can be realized.

Acknowledgments

I am deeply grateful to my advisor Prof. Tomoyuki Yamaguchi for his continual guidance and feedback. I thank my dissertation committee members for all their valuable insights: Prof. Kenji Suzuki, Prof. Itaru Kitahara, Prof. Gaku Shouji, Prof. Masato Tsukada, and Prof. Toshimasa Yamanaka. I would like to express my great appreciation to Prof. Hiromi Mochiyama and all the world-leading professors at the University of Tsukuba for their knowledge in completing this dissertation. I would like to thank all iCE Lab. members and EMP program fellows for their inspiration and friendship. Personal thanks to my family for their support and encouragement throughout my Ph.D. years.

Fundings

I thank all funding, without which the work in this dissertation would not have been possible. Research in Chapter 3, Chapter 4, and Chapter 5 was supported by JSPS KAKENHI Grant-in-Aid for Scientific Research (C) 17K00360, Grant-in-Aid for Scientific Research (B) JP20H02106, and Grant-in-Aid for JSPS Fellows 21J10757. I also graciously thank for financial support to the special fellow in Ph.D. Program in Empowerment Informatics by the University of Tsukuba, and financial support from JSPS Research Fellowship for Young Scientists Program by Japan Society for the Promotion of Science.

References

[1] J. L. Jones, "Robots at the tipping point: the road to iRobot Roomba," *IEEE Robotics & Automation Magazine,* vol. 13, no. 1, pp. 76-78, March 2006. doi: 10.1109/MRA.2006.1598056.

[2] M. Hazas, "Roombas and Landroids: Do Domestic Service Robots Save Energy?," *IEEE Pervasive Computing,* vol. 20, no. 2, pp. 54-57, April-June 2021. doi: 10.1109/MPRV.2021.3067375.

[3] G. Chen, "Robotics Applications at Airports: Situation and Tendencies," *14th International Conference on Measuring Technology and Mechatronics Automation (ICMTMA),* pp. 536-539, 2022. doi: 10.1109/ICMTMA54903.2022.00114.

[4] F. Gigante et al., "Mobile Robotics Experimentation in Industrial Environment," *Interoperability for Enterprise Systems and Applications Workshops 2022,* vol. 3214, p. WS3Paper2, March 2022. https://ceur-ws.org/Vol-3214/WS3Paper2.pdf.

[5] I. Katsamenis et al., "Robotic maintenance of road infrastructures: The heron project," *Proceedings of the 15th International Conference on PErvasive Technologies Related to Assistive Environments,* pp. 628-635, June 2022. doi: 10.1145/3529190.3534746..

[6] K. Nagatani et al., "Design and development of a tethered mobile robot to traverse on steep slope based on an analysis of its slippage and turnover," *2017 IEEE/RSJ International Conference on Intelligent Robots and Systems (IROS),* pp. 2637-2642, 2017. doi: 10.1109/IROS.2017.8206088.

[7] S. Hirose et al., "TITAN VII: quadruped walking and manipulating robot on a steep slope," *Proceedings of International Conference on Robotics and Automation,* vol. 1, pp. 494-500, 1997. doi: 10.1109/ROBOT.1997.620085.

[8] S. Jung et al., "Mechanism and system design of MAV(Micro Aerial Vehicle)-type wall-climbing robot for inspection of wind blades and non-flat surfaces," *2015 15th International Conference on Control, Automation and Systems (ICCAS),* pp. 1757-1761, 2015. doi: 10.1109/ICCAS.2015.7364634.

[9] S. D. Panjaitan et al., "A Drone Technology Implementation Approach to Conventional Paddy Fields Application," *IEEE Access,* vol. 10, pp. 120650-120658, 2022. doi: 10.1109/ACCESS.2022.3221188.

[10] G. Yamauchi et al., "Slip-compensated odometry for tracked vehicle on loose and weak slope," *ROBOMECH Journal,* vol. 4, no. 27, 2017. doi: 10.1186/s40648-017-0095-1.

[11] N. Igo et al., "Robots climbing up and down a steep stairs and robots retrieving objects from high places," *J. Robot. Mechatron.,* vol. 34, pp. 509-522, 2022. doi: 10.20965/jrm.2022.p0509.

[12] S. Shoval, "Stability of a multi tracked robot traveling over steep slopes," *IEEE*

International Conference on Robotics and Automation, vol. 5, pp. 4701-4706, 2004. doi: 10.1109/ROBOT.2004.1302459.

[13] Y. Iwano et al., "Development of the trimmer-type mowing system against a slope," *2016 International Conference on Advanced Mechatronic Systems (ICAMechS),* pp. 23-38, 2016. doi: 10.1109/ICAMechS.2016.7813415.

[14] K. Inoue et al., "Steep slope climbing using feet or shins for six-legged robots," *2015 10th Asian Control Conference (ASCC),* pp. 1-6, 2015. doi: 10.1109/ASCC.2015.7244563.

[15] K. Seo et al., "Design and stability analysis of a novel wall-climbing robotic platform (ROPE RIDE)," *Mechanism and Machine Theory,* vol. 70, pp. 189-208, 2013. doi: 10.1016/j.mechmachtheory.2013.07.012.

[16] J. Bae et al., "Snake robot with driving assistant mechanism," *Applied Sciences,* vol. 10, no. 7478, 2020. 10.3390/app10217478.

[17] G. A. Lynch et al., "A bioinspired dynamical vertical climbing robot," *International Journal of Robotics Research,* vol. 31, no. 8, pp. 974-996, 2012. doi: 10.1177/0278364912442.

[18] G. Gu et al., "Soft wall-climbing robots," *Science Robotics,* vol. 3, no. 25, p. 2874, 2018. 10.1126/scirobotics.aat2874.

[19] J. Xiao et al., "City-Climber: A New Generation Wall-Climbing Robots," *In Climbing and Walking Robots: towards New Application,* pp. 383-402, 2007. doi: 10.5772/5090.

[20] H. Huang et al., "Design and performance analysis of a tracked wall-climbing robot for ship inspection in shipbuilding," *Ocean Engineering,* vol. 131, pp. 224-230, 2017. 10.1016/j.oceaneng.2017.01.003.

[21] P. Beardsley et al., "VertiGo - A Wall-Climbing Robot including Ground-Wall Transition," 29 December 2015. [Online]. Available: https://la.disneyresearch.com/publication/vertigo/. [Accessed 29 December 2022].

[22] W. C. Myeong et al., "Drone-Type Wall-Climbing Robot Platform for Structural Health Monitoring," *6th International Conference on Advances in Experimental Structural Engineering,* August 2015. http://sstl.cee.illinois.edu/papers/aeseancrisst15/213_Myeong_Drone-Type.pdf.

[23] K. Ioi et al., "Experiments and simulations of wall running and transferring of a climbing robot," *2015 International Symposium on Innovations in Intelligent SysTems and Applications (INISTA),* pp. 1-7, 2015. doi: 10.1109/INISTA.2015.7276782.

[24] M. G. Alkalla et al., "A novel propeller-type climbing robot for vessels inspection," *2015 IEEE International Conference on Advanced Intelligent Mechatronics (AIM),* pp. 1623-1628, 2015. doi: 10.1109/AIM.2015.7222776.

[25] M. G. Alkalla et al., "Tele-operated propeller-type climbing robot for inspection of petrochemical vessels," *Industrial Robot,* vol. 44, no. 2, pp. 166-177, 2017. doi:

10.1108/IR-07-2016-0182.

[26] H. Meng et al., "Tire-model-free control for steering of skid steering vehicle," *IEEE Intelligent Vehicles Symposium (IV),* pp. 1590-1595, 2018. 10.1109/IVS.2018.8500612.

[27] P. Veerajagadheswar et al., "S-Sacrr: A staircase and slope accessing reconfigurable cleaning robot and its validation," *IEEE Robotics and Automation Letters,* vol. 7, no. 2, pp. 4558-4565, 2022. doi: 10.1109/LRA.2022.3151572.

[28] S. Ransom et al., "Planetary Rovers with Mecanum Wheels," *10th Workshop on Advanced Space Technologies(ASTRA),* 2008. http://robotics.estec.esa.int/ASTRA/Astra2008/S14/14_04_Ransom.pdf.

[29] F. Adascalitei et al., "Practical applications for mobile robots based on Mecanum wheels – A systematic survey," *Romanian Review Precision Mechanics, Optics and Mechatronics,* pp. 21-29, 2011.

[30] G. Reina, "Cross-coupled control for all-terrain rovers," *Sensors,* vol. 13, pp. 785-800, 2013. doi: 10.3390/s130100785.

[31] J. Qu et al., "Performance analysis and optimization for steering motion mode switching of an agricultural four-wheel-steering mobile robot," *Agronomy,* vol. 12, p. 2655, 2022. doi: 10.3390/agronomy12112655.

[32] S. Mahmood et al., "Propeller-type Wall-Climbing Robots: A Review," *IOP Conference Series: Materials Science and Engineering,* p. 1094, 2021. doi: 10.1088/1757-899X/1094/1/012106.

[33] A. Nishi et al., "Design of a robot capable of moving on a vertical wall," *Advanced Robotics,* vol. 1, no. 1, pp. 33-45, 1986. doi: 10.1163/156855386X00300.

[34] J. Shin et al., "Micro aerial vehicle type wall-climbing robot mechanism," *2013 IEEE RO-MAN,* pp. 722-725, 2013. doi: 10.1109/ROMAN.2013.6628398.

[35] K. Ioi et al., "Development of a compact and rapid wall-climber," *2013 18th International Conference on Methods & Models in Automation & Robotics (MMAR),* pp. 344-349, 2013. doi: 10.1109/MMAR.2013.6669931.

[36] W. C. Myeong et al., "Development of FAROS (Fire-Proof Drone) Using an Aramid Fiber Armor and Air Buffer Layer," *2017 14th International Conference on Ubiquitous Robots and Ambient Intelligence (URAI),* pp. 204-207, 2017. doi: 10.1109/URAI.2017.7992713.

[37] W. Myeong et al., "Development of a Wall-Climbing Drone Capable of Vertical Soft Landing Using a Tilt-Rotor Mechanism," *IEEE Access,* vol. 7, p. 4868–79, 2019. doi: 10.1109/ACCESS.2018.2889686.

[38] K. Sukvichai et al., "Design of a double-propellers wall-climbing robot," *2017 IEEE International Conference on Robotics and Biomimetics (ROBIO),* pp. 239-245, 2017. doi: 10.1109/ROBIO.2017.8324424.

[39] S. K. Mahmood et al., "Novel Wall-Climbing Robot Capable of Transitioning and

Perching," *IOP Conference Series: Materials Science and Engineering (3rd International Conference on Sustainable Engineering Techniques (ICSET 2020)),* vol. 881, p. 012049, 2020. doi: 10.1088/1757-899X/881/1/012049.

[40] S. Tadokoro et al., "The World robot summit disaster robotics category – achievements of the 2018 preliminary competition," *Advanced Robotics,* vol. 33, no. 17, pp. 854-875, 12 June 2019. doi: 10.1080/01691864.2019.1627244.

[41] P. Sekhar et al., "Duct fan based wall climbing robot for concrete surface crack inspection," *2014 Annual IEEE India Conference (INDICON),* pp. 1-6, 2014. doi: 10.1109/INDICON.2014.7030589.

[42] L. Yanget al., "Visual SHM for Concrete Infrastructure Using a Wall-climbing Robot," *Proceedings of the 9th International Conference on Structural Health Monitoring of Intelligent Infrastructure,* pp. 896-901, 4-7 Aug. 2019. https://scholarsmine.mst.edu/cgi/viewcontent.cgi?article=1052&context=inspire-meetings.

[43] J. P. Z. De Paz et al., "Crack detection by a climbing robot using image analysis," *23rd International Conference on Electronics, Communications and Computing (CONIELECOMP 2013),* pp. 87-91, 2013. doi: 10.1109/CONIELECOMP.2013.6525765.

[44] H. Kim et al., "Concrete Crack Identification Using a UAV Incorporating Hybrid Image Processing," *Sensors,* vol. 17, no. 9, p. 2052, 2017. doi: 10.3390/s17092052.

[45] H. Yu et al., "A UAV-based crack inspection system for concrete bridge monitoring," *2017 IEEE International Geoscience and Remote Sensing Symposium (IGARSS),* pp. 3305-3308, 2017. doi: 10.1109/IGARSS.2017.8127704.

[46] S. Nakamura et al., "Inspection test of a tunnel with an inspection vehicle for tunnel lining concrete," *Journal of Robotics and Mechatronics,* vol. 31, no. 6, pp. 762-771, 2019. doi: 10.20965/jrm.2019.p0762.

[47] Y. Takahashi et al., "Velocity control mechanism of the under-actuated hammering robot for gravity compensation," *Proceedings of the International Symposium on Automation and Robotics in Construction,* vol. 34, pp. 1-6, 2017. doi: 10.22260/ISARC2017/0061.

[48] B. L. Luk et al., "Robotic impact-acoustics system for tile-wall bonding integrity inspection," *Mechatronics,* vol. 19, no. 8, pp. 1251-1260, 2009. doi: 10.1016/j.mechatronics.2009.07.006.

[49] F. Inoue et al., "Study on automated inspection robot and quantitative detection of outer tile wall exfoliation by wavelet analysis," *ICCAS 2010,* pp. 994-999, 2010. doi: 10.1109/ICCAS.2010.5669653.

[50] C. J. Salaan et al., "UAV with two passive rotating hemispherical shells and horizontal rotor for hammering inspection of infrastructure," *2017 IEEE/SICE International Symposium on System Integration,* pp. 769-774, 2017. doi:

10.1109/SII.2017.8279315.

[51] C. J. Salaan et al., "Development and Experimental Validation of Aerial Vehicle with Passive Rotating Shell on Each Rotor," *IEEE Robotics and Automation Letters,* vol. 4, no. 3, pp. 2568-2575, July 2019. doi: 10.1109/LRA.2019.2894903.

[52] A. Ichikawa et al., "UAV with manipulator for bridge inspection — Hammering system for mounting to UAV," *2017 IEEE/SICE International Symposium on System Integration,* pp. 775-780, 2017. doi: 10.1109/SII.2017.8279316.

[53] F. Moreu et al., "Remote railroad bridge structural tap testing using aerial robots," *International Journal of Intelligent Robotics and Applications,* vol. 2, pp. 67-80, 2018. doi: 10.1007/s41315-017-0041-7.

[54] P. J. Chun et al., "Utilization of unmanned aerial vehicle, artificial intelligence, and remote measurement technology for bridge inspections," *Journal of Robotics and Mechatronics,* vol. 32, no. 6, pp. 1244-1258, 2020. doi: 10.20965/jrm.2020.p1244.

[55] T. Ikeda et al., "Wall contact by octo-rotor UAV with one DoF manipulator for bridge inspection," *2017 IEEE/RSJ International Conference on Intelligent Robots and Systems,* pp. 5122-5127, 2017. doi: 10.1109/IROS.2017.8206398.

[56] T. Ikeda et al., "Stable impact and contact force control by UAV for inspection of floor slab of bridge," *Advanced Robotics,* vol. 32, no. 19, 2018. doi: 10.1080/01691864.2018.1525075.

[57] B. Li et al., "Wall-climbing robot for non-destructive evaluation using impact-echo and metric learning SVM," *International Journal of Intelligent Robotics and Applications,* vol. 1, pp. 255-270, 2017. doi: 10.1007/s41315-017-0028-4.

[58] T. Iwamoto et al., "Development of testing machine for tunnel inspection using multi-rotor UAV," *Journal of Physics: Conference Series (12th International Conference on Damage Assessment of Structures),* vol. 842, no. 1, p. 012068, June 2017. doi: 10.1088/1742-6596/842/1/012068.

[59] A. Bechar et al., "Agricultural robots for field operations. Part 2: Operations and systems," *Biosystems Engineering,* vol. 153, pp. 110-128, 2017. doi: 10.1016/j.biosystemseng.2016.11.004.

[60] S. Fountas et al., "Agricultural robotics for field operations," *Sensors,* vol. 20, no. 9, p. 2672, 2020. doi: 10.3390/s20092672.

[61] Food and Agriculture Organization of the United Nations (FAO), "Recommendations for Improved Weed Management," *Plant Production and Protection Division,* pp. 1-56, 2006.

[62] T. Bakker et al., "An autonomous weeding robot for organic farming. In Field and Service Robotics," *Field and Service Robotics,* vol. 25, pp. 579-590, 2006. doi: 10.1007/978-3-540-33453-8_48.

[63] I. Daniyan et al., "Development and performance evaluation of a robot for lawn mowing," *Procedia Manufacturing,* vol. 49, pp. 42-48, 2020. doi:

10.1016/j.promfg.2020.06.009.

[64] S. N. Pisharody et al., "Design and Implementation of Bluetooth Controlled Weeder," *2021 Fifth International Conference on I-SMAC (IoT in Social, Mobile, Analytics and Cloud) (I-SMAC),* pp. 1700-1705, 2021. doi: 10.1109/I-SMAC52330.2021.9640936.

[65] B. M. Shiu, "Design of an autonomous lawn mower with optimal route planning," *2008 IEEE International Conference on Industrial Technology,* pp. 1-6, 2008. doi: 10.1109/ICIT.2008.4608497.

[66] M. Song et al., "Path planning for autonomous lawn mower tractor," *Korean Journal of Agricultural Science,* vol. 42, no. 1, pp. 63-71, 2015. doi: 10.7744/CNUJAS.2015.42.1.063.

[67] J. H. Zhou et al., "Research on path planning algorithm of intelligent mowing robot used in large airport lawn," *International Conference on Information System and Artificial Intelligence (ISAI),* pp. 375-379, 2016. doi: 10.1109/ISAI.2016.0086.

[68] C. L. Chang et al., "Integration of Laser scanner and odometry for autonomous robotics lawn mower," *2015 ASABE Annual International Meeting,* 2015. doi: 10.13031/aim.20152190609.

[69] M. Franzius et al., "Embedded robust visual obstacle detection on autonomous lawn mowers," *IEEE Conference on Computer Vision and Pattern Recognition Workshops (CVPRW),* p. 361–369, 2017. doi: 10.1109/CVPRW.2017.50.

[70] M. H. Wu et al., "Study of Autonomous Robotic Lawn Mower Using Multi-Sensor Fusion Based Simultaneous Localization and Mapping," *International Conference on Advanced Robotics and Intelligent Systems (ARIS),* pp. 1-4, 2022. doi: 10.1109/ARIS56205.2022.9910445.

[71] MAFF (Ministry of Agriculture, Forestry and Fisheries), "Summary of the annual report on food, agriculture and rural areas in Japan," 2021. [Online]. Available: https://www.maff.go.jp/e/data/publish/attach/pdf/index-69.pdf. [Accessed 29 December 2022].

[72] The Japanese Association of Rural Medicine (JARM), "Agricultural Accidents that Happened This Way (Koushite okotta nousagyou jiko) (in Japanese)," 2014. [Online]. Available: https://www.maff.go.jp/j/seisan/sien/sizai/s_kikaika/anzen/taimen.html. [Accessed 29 December 2022].

[73] H. Ito et al., "Study on Sideslip Suppression of Weed Cutter Robot with Changing Camber Angle Mechanism for Levee Slope (in Japanese)," *The Proceedings of JSME annual Conference on Robotics and Mechatronics (Robomec),* vol. 2019, pp. 1A1-D07-, 2019. doi: 10.1299/jsmermd.2019.1A1-D07.

[74] K. Iizuka et al., "Study on Reduction of Side Slippage for Cutting Weeding Vehicle with Outrigger Arm (in Japanese)," *The Proceedings of JSME annual Conference on Robotics and Mechatronics (Robomec),* vol. 2022, pp. 1P1-A09-, 2022. doi: 10.1299/jsmermd.2022.1P1-A09.

[75] Y. Nakatsuchi et al., "Development of Grass Cutter Robot for Steep Slope(Robotics and Mechatronics in Agriculture) (in Japanese)," *The Proceedings of JSME annual Conference on Robotics and Mechatronics (Robomec),* vol. 2012, pp. _1A1-H05_1-_1A1-H05_2, 2012. doi: 10.1299/jsmermd.2012._1A1-H05_1.

[76] Y. Iwano et al., "Research Examples of Crawler Mechanism on the Ridge (in Japanese)," *SYSTEMS, CONTROL AND INFORMATION,* vol. 65, no. 12, pp. 483-488, 2021. doi: 10.11509/isciesci.65.12_483.

[77] Y. Uehara et al., "Development of Remote Control Paddy Ridge Mower in Nagano Prefecture (in Japanese)," *SYSTEMS, CONTROL AND INFORMATION,* vol. 65, no. 12, pp. 471-476, 2021. doi: 10.11509/isciesci.65.12_471.

[78] Bullet Real-Time Physics Simulation, "Bullet Real-Time Physics Simulation," [Online]. Available: http://bulletphysics.org. [Accessed 29 December 2022].

[79] R. Smith, "Open Dynamics Engine," [Online]. Available: http://www.ode.org. [Accessed 29 December 2022].

[80] Coppelia Robotics, Ltd., "The robot simulator CoppeliaSim," [Online]. Available: http://www.coppeliarobotics.com. [Accessed 29 December 2022].

[81] H. Mochiyama, "Model validation of discretized spatial closed elastica," *2016 IEEE/RSJ International Conference on Intelligent Robots and Systems (IROS),* pp. 5216-5223, 2016. doi: 10.1109/IROS.2016.7759767.

[82] F. J. Romero-Ramirez et al., "Speeded up detection of squared fiducial markers," *Image and Vision Computing,* vol. 76, pp. 38-47, 2018. doi: 10.1016/j.imavis.2018.05.004.

[83] S. Garrido-Jurado et al., "Generation of fiducial marker dictionaries using mixed integer linear programming," *Pattern Recognition,* vol. 51, pp. 481-491, 2016. doi:10.1016/j.patcog.2015.09.023.

[84] J. Ye et al., "Computerized Hammer Sounding Interpretation for Concrete Assessment with Online Machine Learning," *Sensors,* vol. 18, no. 3, p. 833, 2018. doi: 10.3390/s18030833.

[85] K. Hagiwara et al., "Real-time Defect Detection Method without Training Data for Hammering Test Support System," *2019 IEEE/SICE International Symposium on System Integration (SII),* pp. 205-209, 2019. doi: 10.1109/SII.2019.8700349.

[86] L. J. Y. Kasahara et al., "Acoustic Inspection of Concrete Structures Using Active Weak Supervision and Visual Information," *Sensors,* vol. 20, no. 3, p. 629, 2020. doi: 10.3390/s20030629.

[87] Y. F. Shih et al., "Improving Non-Destructive Test Results Using Artificial Neural Networks," *International Journal of Machine Learning and Computing,* vol. 5, no. 6, pp. 480-483, 2015. http://www.ijmlc.org/vol5/557-X022.pdf.

[88] T. Fukumura et al., "A Study on Hammering Test using Deep Learning," *2020 IEEE 15th International Conference of System of Systems Engineering (SoSE),* pp. 261-

264, 2020. doi: 10.1109/SoSE50414.2020.9130517.

[89] MathWorks, Inc, "Classify Sound Using Deep Learning," [Online]. Available: https://mathworks.com/help/audio/gs/classify-sound-using-deep-learning.html. [Accessed 29 December 2022].

[90] S. Higa et al., "Measurement of stress distributions of a wheel with grousers traveling on loose soil," *2016 IEEE International Conference on Robotics and Automation (ICRA),* pp. 2828-2833, 2016. doi: 10.1109/ICRA.2016.7487445.

[91] M. Brandão et al., "Friction from vision: A study of algorithmic and human performance with consequences for robot perception and teleoperation," *2016 IEEE-RAS 16th International Conference on Humanoid Robots (Humanoids),* pp. 428-435, 2016. doi: 10.1109/HUMANOIDS.2016.7803311.

[92] S. Kiribayashi et al., "Position estimation of tethered micro unmanned aerial vehicle by observing the slack tether," *2017 IEEE International Symposium on Safety, Security and Rescue Robotics (SSRR),* pp. 159-165, 2017. doi: 10.1109/SSRR.2017.8088157.

[93] L. Martelloni et al., "Assessment of the Cutting Performance of a Robot Mower Using Custom Built Software," *Agronomy,* vol. 9, no. 5, p. 230, 2019. doi: 10.3390/agronomy9050230.

[94] J. Yang et al., "Omnidirectional-vision-based estimation for containment detection of a robotic mower," *2015 IEEE International Conference on Robotics and Automation (ICRA),* pp. 6344-6351, 2015. doi: 10.1109/ICRA.2015.7140090.